

# **Radiocarbon signature of dissolved organic carbon (DOC) in arctic rivers**

-

## **An evaluation of DOC extraction methods and a Lena Delta case study**

Master Thesis  
MSc Programme Marine Geosciences  
Department of Geosciences  
University Bremen

By  
**Hendrik Grotheer**

1<sup>st</sup> supervisor: Prof. Dr. Gesine Mollenhauer  
2<sup>nd</sup> supervisor: Prof. Dr. Boris Koch

**Bremen, 2012**

***“I am among those who think that science has great beauty. A scientist in his laboratory is not only a technician: he is also a child placed before natural phenomena which impress him like a fairy tale.”***

Marie Curie, 1867-1934

## Table of Contents

<b>1. Abstract</b> .....	- 3 -
<b>2. Introduction</b> .....	- 4 -
<b>3. Materials and methods</b> .....	- 7 -
3.1 Radiocarbon background.....	- 7 -
3.2 Method evaluation.....	- 8 -
3.2.1 <i>Materials</i> .....	- 8 -
3.2.2 <i>DOC concentration</i> .....	- 9 -
3.2.3 <i>Extraction methods</i> .....	- 9 -
3.2.4 <i>Radiocarbon measurements</i> .....	- 17 -
3.3 Lena Delta.....	- 19 -
<b>4. Results</b> .....	- 21 -
4.1 Extraction efficiency.....	- 21 -
4.2 <sup>14</sup> C analyses .....	- 23 -
4.4 Lena Delta.....	- 25 -
<b>5. Discussion</b> .....	- 26 -
5.1 Introduction to blank carbon determination and correction .....	- 26 -
5.2 Blank carbon determination and correction .....	- 28 -
5.2.1 <i>Ultraviolet-oxidation</i> .....	- 28 -
5.2.2 <i>Roto-evaporation</i> .....	- 30 -
5.2.3 <i>Blank correction for RV and UV</i> .....	- 31 -
5.2.4 <i>Solid phase extraction</i> .....	- 33 -
5.3 Lena Delta.....	- 41 -
5.3.1 <i>Blank correction and data reliability</i> .....	- 41 -
5.3.2 <i>Origin of organic matter in the Lena Delta</i> .....	- 41 -
5.3.3 <i>Fate of DOC along the Lena River</i> .....	- 43 -
5.3.4 <i>Arctic river DOC and thawing permafrost</i> .....	- 46 -
<b>6. Conclusion</b> .....	- 50 -
<b>7. Acknowledgments</b> .....	- 53 -
<b>Appendix</b> .....	I

## 1. Abstract

Riverine discharge of dissolved organic carbon (DOC) represents an important part of the global carbon cycle. Substantial effort is being invested to determine fluxes, composition and isotopic signature of terrestrial DOC to the oceans and its influence on climate change. However, all predictions of the climate change are depending on the quality of the data that's being used. Unfortunately, there is a severe lack of knowledge about the DOC data quality, due to under-investigated methodological constraints during riverine DOC sample processing. The first part of this thesis compares three extraction methods commonly used to determine the stable and radiogenic carbon signature of DOC. Ultraviolet-oxidation, roto-evaporation and solid phase extraction were compared to unravel blank carbon incorporation, data reliability and methodological limitations.

Ultraviolet-oxidation shows small blank incorporation but provides most reliable bulk  $\text{DO}^{14}\text{C}$  data. The roto-evaporation results in smallest blank carbon incorporation but also the removal of non-polar low-molecular-weight components. However, this does not alter the bulk  $\text{DO}^{14}\text{C}$  signature for samples from temperate and arctic regions. The roto-evaporation has been proven to be an inexpensive and reliable alternative to the ultraviolet-oxidation. Solid phase extraction showed highest blank carbon incorporation and additionally discrimination against the bioactive fraction of DOC. Uncertainties about the blank incorporation and the removal of the important bioactive DOC makes the solid phase extraction an inappropriate method to extract riverine DOC.

The second part applies the roto-evaporation method to a set of Lena Delta (northeast Siberia) samples in preparation for  $\text{DO}^{14}\text{C}$  measurements. Stable and radiogenic isotopy reveals that the DOC in the Delta originates from local litter leaching and near-surface chemical weathering of Holocene soils. Upstream DOC is being removed en route to the Delta, suggesting that the majority of export carbon to the Arctic Ocean originates from coastal-near regions. Progressive isotopic depletion of coastal near  $\text{DO}^{14}\text{C}$  during the late season suggests increasing permafrost thawing in response to global warming. The increase in thawing depth is highest close to the Arctic Ocean and is weakened towards the Siberian hinterland. However, no such trend could be observed for North American permafrost suggesting that Siberian permafrost and climate response faster to and will be more influenced by ongoing climate changes.

## 2. Introduction

The global carbon cycle is defined by the interaction between various organic and inorganic carbon reservoirs on Earth, including the atmosphere, oceans, terrestrial soils, biosphere and marine biota, as well as fossil carbon present as kerogen, fossil fuels, sedimentary rocks and the Earth's crust. Long- and short-term variations of carbon transfer processes between these carbon pools ultimately define the atmospheric carbon dioxide composition and thus regulate the global climate [Hedges 1992]. Investigating the present carbon cycle became a topic of interest since the effects of human activity on the global atmospheric composition, like enhanced emission of CO<sub>2</sub> in response to the globally increasing energy demand by burning fossil fuels. The related climatic changes remain ill-constrained and probably underestimated.

Oceanic dissolved organic carbon (DOC) is an important part of the global carbon cycle. It is the largest pool of organic material in the ocean ( $0.6 \times 10^{18}$  gC) and is comparable in size to atmospheric carbon dioxide. Operationally DOC is characterized as the fraction of organic matter soluble in water that fits through a 0.45 µm filter [Hedges 1992].

Although DOC is a subject of research for nearly a century, its molecular composition and global-, as well as small-scale cycling remains poorly understood. Global riverine input of ~0.2 Gt DOC per year [Meybeck 1982] reflects an important source for oceanic DOC, but the majority is believed to originate from primary production in the euphotic zone [Williams & Gordon 1970]. However, human activity is believed to change global carbon pools and fluxes in between. As a result of burning fossil fuels, modifying the land surface and increased cattle breeding billions of tonnes of carbon greenhouse gases are exposed into the atmosphere and changing its heat-trapping capacity, hence changing Earth's climate [IPCC 2007]. Although the modern increase in the atmospheric carbon pool is directly linked to human activity, models suggest naturally enhanced atmospheric carbon enrichment in the future [Friedlingstein *et al.* 2006]. The degree of future carbon enrichment in the atmosphere depends on the response of terrestrial and ocean systems to the mankind stimulated climate change [Friedlingstein *et al.* 2006]. Terrestrial response processes e.g. are thawing permafrost or wetland drying [Field & Raupach 2004]. Thawing permafrost in response to global warming for example would lead to remobilization of old, previously stabilized carbon [Neff *et al.* 2006], hence an increase in riverine fluxes of terrestrial carbon towards the ocean. Increased riverine carbon import into the ocean will ultimately enhance the flux of carbon dioxide from the ocean to the atmosphere and thus amplifying the greenhouse effect. Therefore tracing riverine DOC fluxes and understanding riverine DOC cycling dynamics became an intensified research subject during the last decades.

Due to improved analytical techniques, recent studies showed that DOC mainly consists of lignin phenols, lipids, highly oxygenated aromatic and nitrogen-bearing compounds [Koch *et*

*al.* 2005; *Schmidt et al.* 2009]. The molecular composition of DOC in various reservoirs provides information about its source and allows further investigation of its cycling processes. An irreplaceable tool to further analyse DOC cycling and fluxes are  $^{14}\text{C}$  isotope signatures of the dissolved organic matter.  $^{14}\text{C}$  signatures of DOC in combination with stable carbon isotope data ( $\delta^{13}\text{C}$ ), for example, enable the identification of sinks and sources of DOC within a regime [*Raymond & Bauer* 2001a].

However, the applicability of  $\text{DO}^{14}\text{C}$  and  $\text{DO}^{13}\text{C}$  data is limited by the quality of the data. Unfortunately, there is a severe lack of knowledge about the DOC data quality, due to under-investigated methodological constraints during riverine DOC sample processing.

Isotope analyses on DOC require the isolation of the organic matter from its medium and the conversion to carbon dioxide. Several methods including freeze-drying (FD), roto-evaporation (RV) or ultra-filtration are available to extract DOC from the water and have been used predominantly to analyse riverine DOC. Analyses on marine DOC are limited due to overwhelming methodological difficulties, associated with low DOC concentration, high salt content and high blanks [*Beaupré et al.* 2007].

Nevertheless, two recently developed methods promise improvements in  $\text{DO}^{14}\text{C}$  preparation. Using ultraviolet light (UV) for a direct photo oxidation of DOC to carbon dioxide showed very high extraction efficiency along with low blank contaminations [*Beaupré et al.* 2007]. The UV-oxidation is believed to be non-selective for certain compound classes during  $\text{CO}_2$  generation and the analysed  $^{14}\text{C}$  signature, therefore, reflects bulk  $\text{DO}^{14}\text{C}$ . However, setting up of a UV-oxidation system is very cost intensive [*Beaupré et al.* 2007] and may not be affordable for smaller work groups.

In addition, a simple solid-phase extraction (SPE) of DOC, using a styrene divinyl benzene polymer- (PPL) cartridge, enables inexpensive, fast and robust in-field DOC sampling [*Dittmar et al.* 2008]. SPE furthermore enables additional analysis like DOC quantification, separation by LC-MS and characterization by FT-ICR-MS [*Peterson et al.* 2003; *Dittmar et al.* 2008; *Koch et al.* 2008]. Unfortunately, SPE shows low extraction efficiencies, about 65 % for riverine and 43 % for marine samples [*Dittmar et al.* 2008]. Nevertheless, *Flerus et al.*, [2011] presented  $^{14}\text{C}$  ages for deep marine DOC similar to previous studies by *Bauer et al.*, [1992] suggesting that the loss of organic matter during the extraction does not effect the  $^{14}\text{C}$  signature significantly. However, it remains unclear how the SPE influences the  $\text{DO}^{14}\text{C}$  signature in other, more complex, environments.

The first part of this thesis compares three extraction methods commonly used to determine the stable and radiogenic carbon signature of DOC. Ultraviolet-oxidation (UV), roto-evaporation (RV) and solid phase extraction (SPE) are compared to unravel blank carbon incorporation, data reliability and methodological limitations to provide enhanced insights into data quality and inter-methodological comparability.

As northern latitudes are believed to be most vulnerable to the climate change [IPCC 2007], the second part of this thesis focuses on riverine DOC in the Arctic region. Huge areas of the northern hemisphere are currently covered by permafrost, in total about 16% of all global soils, containing about 1672 Pg carbon in the upper 3 m [Tarnocai *et al.* 2009]. This huge reservoir of organic carbon contains about 50 % of all organic carbon stored in global soils and is believed to be highly sensitive to climatic changes [Schuur *et al.* 2008; Tarnocai *et al.* 2009]. Models predict increasing temperature in the northern circumpolar region of 7 to 8 °C during the next century [IPCC 2007]. As a consequence, thawing permafrost and the release of fossil organic material, as well as the resulting microbial decomposition of previously frozen organic carbon is one of the most important feedback mechanisms of the terrestrial ecosystem to the atmosphere. The dynamics of permafrost thawing as a result of increasing temperature and the effects of remobilized fossil carbon on atmospheric carbon dioxide composition and, thus, the global climate remain poorly understood and under-investigated. Nevertheless, various studies showed that northern hemisphere permafrost already experienced major changes during the second half of the 20<sup>th</sup> century. Due to widespread and increasing boreal warming [Serreze *et al.* 2000; Giorgi *et al.* 2001] increased freshwater discharge from Arctic regions to the Arctic ocean has been observed [Peterson *et al.* 2002] as well as a decline in permafrost extent [Serreze *et al.* 2000; Jorgenson *et al.* 2001]. Very little is known so far about the age, composition, seasonal variations and fate of DOC transported by Arctic rivers. Therefore, Neff *et al.*, [2006] published a first dataset investigating the DOC composition and age over an entire year for the Kolyma river, East Siberia. The bulk of the annual DOC flux was modern in origin ( $\Delta^{14}\text{C} > 100 \text{ ‰}$ ; fMC > 1) containing high concentrations of terrestrial lignin monomers, suggesting primarily surface leaching during the spring thaw. Towards the end of the summer however, much smaller concentrations of lignin were measured and radiocarbon ages became significantly older ( $\Delta^{14}\text{C} < 0 \text{ ‰}$ ; fMC < 1) indicating remobilization of stabilized carbon from probably deeper soil horizons [Neff *et al.* 2006]. However, they were not able to show whether or not these observations are a local phenomenon or can be extrapolated to the entire Arctic regime. To obtain a better understanding of the fate of DOC in Arctic rivers, the extent of permafrost thawing, carbon mobilization dynamics and the resulting climatic implications this thesis presents isotope analyses of DOC samples from the Lena Delta, northeast Siberia (Fig. 1). The Lena Delta represents the largest delta of the circum-polar landmasses and is formed by the 4400 km long Lena River. The river discharges about 581 km<sup>3</sup>/yr water [Holmes *et al.* 2011] and contributes about 35.5 % ( $6.47 \times 10^{12}$  g/yr) of the total riverine DOC flux towards the Arctic Ocean [Amon *et al.* 2012]. This makes the Lena River and adjacent Delta an immanently suitable location to investigate small- and large-scale carbon dynamics and their implications for the global carbon cycle.

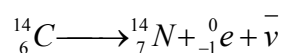
### 3. Materials and methods

#### 3.1 Radiocarbon background

Carbon naturally occurs as three isotopes, atoms with the same number of protons but varying number of neutrons and thus a different atomic weight: stable isotopes  $^{12}\text{C}$  (98.89 %) and  $^{13}\text{C}$  (1.11 %), and the cosmogenic nuclide  $^{14}\text{C}$  ( $1.176 \times 10^{-12}$  %). The radioisotope  $^{14}\text{C}$  is constantly produced in the lower stratosphere by collisions between low-energy cosmic ray neutrons and atmospheric nitrogen atoms ( $^{14}\text{N}$ ); a process during which a proton is emitted.



The produced  $^{14}\text{C}$  is rapidly oxidised to  $^{14}\text{CO}$  and  $^{14}\text{CO}_2$  and mixed within the atmosphere. Via photosynthesis the  $^{14}\text{C}$  enters the terrestrial and marine biosphere either by uptake of atmospheric  $\text{CO}_2$  or is implemented as dissolved inorganic carbon (DIC) into plant biomass [Damon *et al.* 1978]. During its lifetime, organisms remain in isotopic equilibrium with the atmosphere due to the quick exchange processes between biomass and atmosphere. As soon as the organisms die, the concentration of  $^{14}\text{C}$  within the plants tissue constantly declines as result of the natural decay of the radioactive isotope. The  $^{14}\text{C}$  incorporated into the biomass decays into atomic nitrogen through the emission of  $\beta$ -particles and antineutrinos with a half-life of 5.730 years.



Therefore, measuring the remaining  $^{14}\text{C}$  concentration of a carbon containing sample allows the calculation of the age of the organic material by comparing it to the  $^{14}\text{C}$  concentration of a standard material with known age. These days, the three natural carbon isotopes can be separated by accelerated mass spectrometry (AMS) using the atomic weight differences of the isotopes, allowing the  $^{14}\text{C}/^{12}\text{C}$  ratio to be reported. By comparison to a modern standard material with the  $^{14}\text{C}$  isotopic signature of the year 1950, i.e. a standard prior to the artificial enrichment of  $^{14}\text{C}$  in the atmosphere introduced by nuclear bomb testing, final results are reported as fraction modern carbon ( $f\text{MC}$ ). The modern standard  $^{14}\text{C}/^{12}\text{C}$  ratio is defined as 95% of the activity of the International Atomic Energy Agency oxalic acid II standard. The fraction modern carbon is calculated as follows [Stuiver & Polach 1977]:

$$fMC = \left( \frac{{}^{14}\text{C}/{}^{12}\text{C}_{\text{sample}}}{{}^{14}\text{C}/{}^{12}\text{C}_{\text{standard}}} \right) \quad (1)$$

To enable the comparison between samples from different environments, by accounting for isotopic fractionation, the  ${}^{14}\text{C}/{}^{12}\text{C}$  ratio of a sample is normalized to a  $\delta^{13}\text{C}$  value of -25 ‰ relative to the Vienna PeeDee Belemnite (VPDB), which is equivalent to the  ${}^{13}\text{C}$  composition of terrestrial wood. The correction is calculated as follows [Stuiver & Polach 1977]:

$${}^{14}\text{C}/{}^{12}\text{C}_{\text{sample},\delta^{13}\text{C}} = {}^{14}\text{C}/{}^{12}\text{C}_{\text{sample}} \times \left( \frac{(1 - 25/1000)}{(1 + \delta^{13}\text{C}/1000)} \right)^2 \quad (2)$$

Additionally, the modern standard is adjusted to a value of pre-industrial wood in the year 1890 containing no fossil fuel-derived carbon [Karlén *et al.* 1968] by normalizing to a  $\delta^{13}\text{C}$  value of -19 ‰VPDB. The correction is calculated as follows [Stuiver & Polach 1977]:

$${}^{14}\text{C}/{}^{12}\text{C}_{\text{standard},\delta^{13}\text{C}} = 0.95 \times {}^{14}\text{C}/{}^{12}\text{C}_{\text{standard}} \times \left( \frac{(1 - 19/1000)}{(1 + \delta^{13}\text{C}/1000)} \right)^2 \quad (3)$$

## 3.2 Method evaluation

### 3.2.1 Materials

A set of different standard materials with varying, but known  $fMC$  values were used to determine the amount of blank carbon, external carbon introduced into the sample during sample processing, and extraction efficiencies of the different DOC extraction methods (Tab. 1). Chemical structures and properties of the standards are shown in the appendix (A-I). The commonly used and well known isotopically dead (glycine hydrochloride;  $fMC_{\text{Gly}} = 0$ ) and isotopically modern (oxalic acid;  $fMC_{\text{Ox}} = 1.2933$ ) standards were used for all methods. Additionally, two lignin phenol standards (*p*-coumaric acid;  $fMC_{\text{p-Coum}} = 0.0101$  and 4-hydroxybenzaldehyde;  $fMC_{\text{4-Hydroxy}} = 0.0012$ ) were concentrated from an aqueous phase by solid phase extraction. In order to simulate arctic river properties solutions with 300-500  $\mu\text{MC}$  were prepared in suprapur  $\text{H}_2\text{O}$  (EMSURE water for analysis, MERCK) and ~20 mL replicates were stored refrigerated (~4 °C) in high-density polyethylene (HDPE) bottles. In addition, natural river water was collected in February 2012 from the Cow Creek (53°06'N 8°50'E) near the MPI building at the University Bremen, Germany in February 2012. The

water was filtered through a pre-combusted 0.45  $\mu\text{m}$  glass fiber filter (*WHATMAN*) and acidified with concentrated hydrochloric acid (HCl) and also stored in  $\sim 20$  mL replicates. Cow Creek DOC samples were extracted by all three methods to investigate how the extraction method affects the analyzed isotopic signature of a natural sample.

All used glassware and plastic utilities were either pre-combusted (5 h at 450  $^{\circ}\text{C}$ ) or cleaned for at least 24 h in a 10 % hydrochloric acid (HCl) solution and rinsed with deionized  $\text{H}_2\text{O}$  (*SERALPUR*) right before usage.

Standard material		$fMC_{std}$	$\sigma fMC_{std}$	Reference
oxalic acid	NIST SRM 4990C	1.2933	0.001	[ <i>Mann</i> 1983]
glycine hydrochloride	Sigma G2879	0	0	n.a.
<i>p</i> -coumaric acid	Sigma C90008-5G	0.0101	0.0005	[ <i>Mollenhauer</i> unpubl.]
4-hydroxybenzaldehyde	Aldrich 14,408-8	0.0012	0.0003	[ <i>Mollenhauer</i> unpubl.]

**Tab. 1:** Summary of used standards during the method evaluation with initial fMC values and corresponding uncertainties.

### 3.2.2 DOC concentration

Initial DOC concentrations of the standard solutions and natural samples were determined at the AWI in Bremerhaven, Germany. Aliquots of 6.5 mL sample were acidified in the auto-sampler of a *Shimadzu TOC-VCPN* analyzer and subsequently measured directly by high temperature catalytic oxidation in the same instrument. Recorded values were quantified according to an external calibration and corrected for the Deep Sea Reference Standard (DSR) material supplied by D. Hansell (University of Miami, Florida). The mean of five replicate measurements are reported here with a precision better than  $\pm 2$   $\mu\text{MC}$ .

### 3.2.3 Extraction methods

#### *Roto-evaporation (RV)*

The simplest way to remove large volumes of water without an accompanied loss of dissolved constituents is to evaporate the water. All dissolved components, e.g. salts, organic matter and micronutrients will then remain as a dry residue. A *LABORATA (Heidolph)* roto-evaporation equipment was used at constant temperature and pressure (50  $^{\circ}\text{C}$ , 70 mbar,  $\Delta P=20$  mbar). Samples were filled into 50 mL pear shaped flasks and evaporated. The residue was redissolved in 4 mL suprapur  $\text{H}_2\text{O}$  and transferred into 4 mL screw cap vials. The samples were subsequently dried under a stream of nitrogen gas ( $\text{N}_2$ ) at

50 °C and stored refrigerated. In between samples the equipment was cleaned by evaporating 50 mL seralpur H<sub>2</sub>O to avoid cross-contamination.

### Solid phase extraction (SPE)

According to the solid phase extraction scheme proposed by *Dittmar et al.* [2008], 1 g PPL-cartridges (*Varian Bond*) with ~3 mL volume were used to extract DOC from aqueous solution. The sorbent material, PPL (styrene divinyl benzene polymer), with a pore size of 150 Å is capable to adsorb highly polar to non-polar substances from large volumes of water. Cartridges were placed in MeOH (methanol, distilled twice) for 24 h prior usage to remove any contamination. Immediately before loading with the sample, the cartridges were additionally rinsed with 2 cartridge volumes (4–6 mL) of MeOH and acidified suprapur H<sub>2</sub>O ( $pH = 2-3$ ) each. For the DOM adsorption, the sample was loaded on the cartridge continuously with glass pipettes and allowed to pass through by gravity. Afterwards, the cartridge was rinsed with 2 cartridge volumes of acidified suprapur H<sub>2</sub>O for complete removal of remnant salts. Following the salt removal, the sorbent was dried under a stream of N<sub>2</sub> for ~45 min. Then 4 mL of MeOH was used to immediately elute the adsorbed DOM into a 4 mL screw cap vial. The eluant was finally dried under a stream of N<sub>2</sub> at 50 °C and stored refrigerated. The process is illustrated in Fig.1.

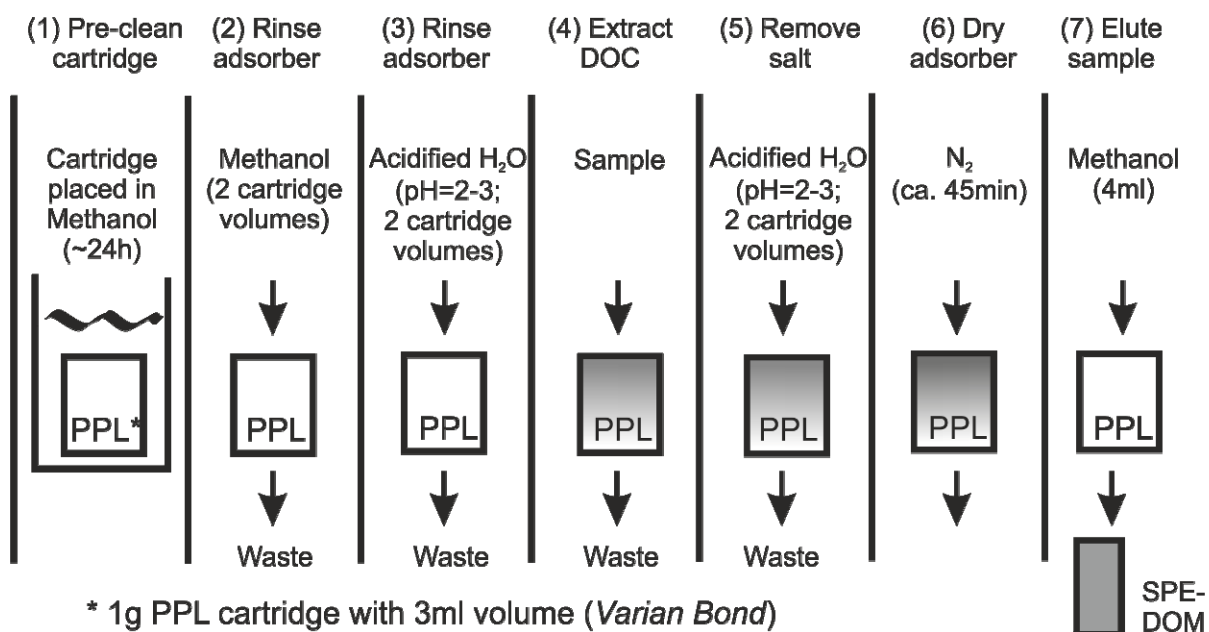
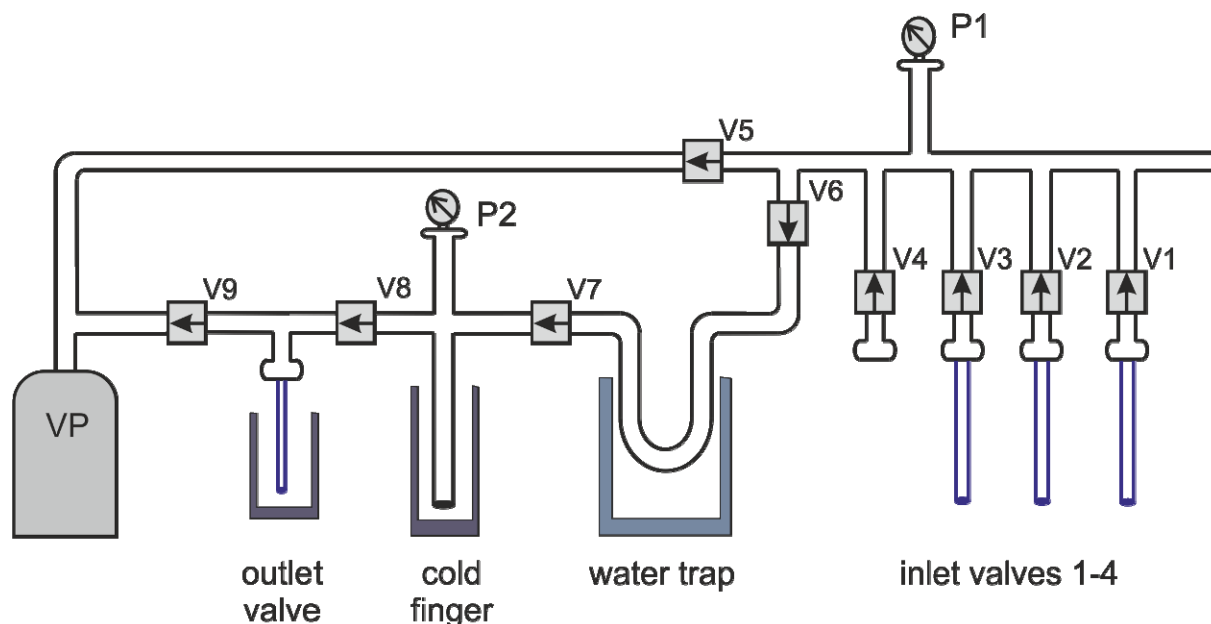


Fig. 1: Scheme of the solid phase extraction procedure (Modified after *Dittmar et al.* [2008]).

## <sup>14</sup>C analysis preparation

### CO<sub>2</sub> generation



**Fig. 2:** Configuration of the vacuum-line system at the University Bremen, Germany (VLB). V1 to V7 are flip valves (*SWAGELOK*) to separate individual parts of the vacuum-line. Inlet valves 1–4 are screw-on valves (*SWAGELOK*) to connect 9 mm outer diameter (OD) quartz tubes and cracker to the vacuum-line. P1 is the first pressure transducer (Pirani transducer, measuring range  $1.3 \times 10^{-5}$  to 1000 mbar (*ILMVAC*)). P2 is the second pressure transducer (Piezo/Pirani transducer, measuring range  $1.3 \times 10^{-5}$  to 2000 mbar (*ILMVAC*)). VP is the vacuum pump.

To enable <sup>14</sup>C analysis the extracted organic material needs to be converted to carbon dioxide (CO<sub>2</sub>) by high temperature oxidation. The process is explained in the following, based on the vacuum-line system used at the University Bremen, Fachbereich 5, Laboratories of Prof. Dr. Mollenhauer (Fig. 2; in the following referred to as VLB).

The complete extracts were transferred either with 3 x 125 µL MeOH (SPE) or 4 x 125 µL suprapur H<sub>2</sub>O (RV) into pre-combusted (5 h at 900 °C) quartz tubes (7 cm x 6 mm) and dried under a stream of N<sub>2</sub> at 50 °C. The dried quartz tubes were filled with 300 mg pre-combusted (5 h at 900 °C) granulated copper(II)oxide (CuO for elemental analysis; *MERCK*) as an oxidizing agent and sealed with a small ball of pre-combusted (5 h at 900 °C) silver wool (Ag for elemental analysis; *ELEMENTAR*) to bind potentially present organohalogens on the silver surface. The small quartz tubes were subsequently cleaned on the outside with dichloromethane (DCM) and MeOH, and placed in larger pre-combusted (5 h at 900 °C) quartz tubes (26 cm x 9 mm) that were then immediately connected to one of the inlet valves 1–4 (Fig. 2). During the CO<sub>2</sub> generation preparation step, valves V6–V9 are closed and V5 is open. Therefore, the line is evacuated between valves V1-V4 and the vacuum pump (VP).

The lower end of the connected quartz tubes were placed in a slush of ethanol and dry ice ( $T \approx -78^{\circ}\text{C}$ ) to freeze-trap all organic components except atmospheric CO<sub>2</sub>. The tubes were subsequently evacuated to a minimum pressure of  $P_1 = 1 \times 10^{-5}$  mbar (as read from

pressure transducer P1) by opening the corresponding valves (V1–4) to remove all atmospheric volatile gases like CO<sub>2</sub>, N<sub>2</sub> and H<sub>2</sub>O. Once the minimum pressure was reached, the corresponding valves (V1–4) were closed. A leak check was performed by reopening the valve after ~30 sec which was passed, if the pressure remained constant at the previously recorded minimum value. After passing the leak check and closing the valve, the slush was replaced by a liquid nitrogen bath ( $T \approx -196^{\circ}\text{C}$ ) and the quartz tubes were finally flame sealed with a hydrogen/oxygen torch.

Afterwards, the sealed quartz tubes were baked at 900 °C for 5 h during which all organic material was oxidized to CO<sub>2</sub> and H<sub>2</sub>O, and, depending on the initial sample, minor traces of nitrogen oxides (NO<sub>x</sub>) and sulfur oxides (SO<sub>x</sub>). The added CuO and the high temperatures lead to a complete oxidation of the organic material and no generation of carbon monoxide (CO) was expected.

### *CO<sub>2</sub> purification and quantification*

Radiocarbon analyses require pure CO<sub>2</sub> therefore the gas mixture generated during the baking process needs to be cleaned and the amount of purified CO<sub>2</sub> must be quantified. The general approach to purify gas mixtures is to pass the gas stream through a series of cold traps within a vacuum-line with different temperatures, where, depending on the freezing point, the individual gases are fixated and isolated from each other. The entire process will be explained based on the vacuum-line in Bremen (Fig. 2). Since only the CO<sub>2</sub> is of interest to us, the vacuum-line set up that was used was simpler and just utilized 2 cold traps, one to remove the water and one to fixate the CO<sub>2</sub>.

During the purification and quantification valve V5 remains closed. The sample containing quartz tube was placed in a “cracker” and connected to the vacuum-line (inlet valve 1–4) and a 15 cm x 6 mm *Durex* tube was connected to the outlet valve. By opening the corresponding valves (V1–4) and valves V6 to V9 the vacuum line and cracker were evacuated to the minimal pressure ( $P_1 \approx 4 \times 10^{-4} \text{ mbar}$ ) being able to remove all atmospheric gases (reading off pressure transducer P1). As the minimum pressure was obtained, the corresponding inlet valve (V1–4) was closed, leak checked and the sample quartz tube was finally cracked. Simultaneously V7 was closed and the U-shaped water-trap was immersed in the ethanol/dry ice slush. By opening the corresponding inlet valve (V1-4) the gas stream passes through the line and, inadvertently gases like H<sub>2</sub>O or NO<sub>x</sub> were fixated in the water-trap. As soon as P1 was stabilized the cold finger was immersed in liquid nitrogen and V8 was closed. By opening V7 for three minutes, all CO<sub>2</sub> was fixated in the cold-finger. The cold finger has a constant volume and is connected to a second pressure transducer (P2). Three minutes is sufficient time, giving the inner diameter and length of the vacuum-line, for all CO<sub>2</sub> to be

fixated in the cold-finger without diffusive isotopic fractionation. After three minutes, V8 was re-opened for ~30 sec to remove all residual volatile gases from the vacuum-line. Afterwards, V7 and V8 were closed and the liquid nitrogen bath was replaced by ethanol/dry ice slush. As soon as the cold-finger was in equilibrium with the slush temperature and P2 had stabilized, the resulting pressure was used for the CO<sub>2</sub> quantification. Afterwards, the *Durex* tube, connected to the outlet valve, was embedded in liquid nitrogen and V9 was closed. By opening V8 for 2 min, all CO<sub>2</sub> from the cold finger was freeze-trapped in the *Durex* tube. After 2 mins elapsed, V9 was opened shortly to remove remaining volatile gases. Afterwards, the sample containing *Durex* tube was flame sealed.

The sealed *Durex* tubes were sent for <sup>14</sup>C analysis to the National Ocean Sciences Accelerator Mass Spectrometry (NOSAMS) facility at the Woods Hole Oceanographic Institution (WHOI) in Woods Hole, Massachusetts, USA.

The volume of the cold-finger of the vacuum-line in Bremen is not known; therefore the amount of CO<sub>2</sub> must be quantified based on an external calibration. For the calibration various gas standards, with known CO<sub>2</sub> concentrations were used and subsequently introduced into the line and fixated in the cold-finger following the previously described procedure. According to the ideal gas law (Eq. 4), the resulting pressures (P2) should be proportional to the amount of introduced CO<sub>2</sub>. Unfortunately no linear correlation between pressure and sample amount could be observed, most likely due to an inappropriate relation between cold-finger volume and measuring range of the pressure transducer. The non-linear relation between pressure and sample amount causes uncertainties for the quantification of sample CO<sub>2</sub>. These uncertainties are negligible when the quantification is used to provide rough sample amounts for further isotopic analyses. However, the quantification is too imprecise to use the calculated amounts for exact blank carbon calculations. Since very accurate quantification of the sample amounts was mandatory for this MSc project, the purification and quantification were performed on two other, more precise vacuum-lines. Samples were purified and quantified on the vacuum-line system at the Glaciology working group at the Institut für Umweltphysik (IUP) of the University Heidelberg, Germany, in the following referred to as VLH, and on the vacuum-line system at the NOSAMS facilities at WHOI (VLWH). The setup of both vacuum-lines is slightly different than VLB but follows the same general procedure. Both lines are equipped with a well-defined manometric volume (cold-finger) and corresponding pressure transducer with uncertainties better than ±0.2mbar.

### *Ultraviolet-oxidation (UV)*

The ultraviolet-oxidation of the organic matter and direct conversion to CO<sub>2</sub> was performed at the NOSAMS facilities at WHOI according to the method and setting proposed by Beaupré et al. (2007). A detailed description of the instrumental setting can be found in Beaupré et al. (2007) but the general setting will be explained in the following. Construction plans, descriptions and pictures are shown in the appendix (Fig. A-1–A-4).

### *UV-reactor and DOC vacuum-line setting*

The UV-reactor consists of three main parts: (1) the photochemical reactor and corresponding heat exchanger (Fig. A-1); (2) the UV-lamp and reflector (Fig. A-2); and (3) the reaction chamber (Fig. A-3).

The photochemical reactor body (1) is a custom UV-transparent vitreous silica cylinder with an internal volume of ~1 L, necked down to a 65/40 spherical joint (SJ) socket-member. A custom *Pyrex*-encased magnetic spin bar inside the photochemical reactor ensures continuous mixing of the water and an even irradiation. The *Pyrex* heat exchanger is a cold-finger condenser, connected to the reactor via a 65/40 SJ ball-member lubricated with 85 % phosphoric acid (H<sub>3</sub>PO<sub>4</sub>) and secured with stainless steel screw-lock pinch clamps. The heat exchanger serves as a helium gas inlet to the reactor, CO<sub>2</sub> gas outlet to the vacuum-line and to cool the sample during irradiation through a closed cooling water cycle. The *Pyrex* helium tubing is connected by an Ultra-Torr (*SWAGELOCK*) fitting, whereas 18/9 SJ sockets connect the recirculation chiller's (5 °C) cooling water via polyvinyl chloride (PVC) tubing (*Nalgene*) over 18/9 SJ o-ring ball-members, secured with stainless steel screw-lock pinch clamps, with the heat exchanger. The CO<sub>2</sub> outlet is connected via an 18/9 SJ socket and o-ring ball-member over *Pyrex* tubing to the adjacent vacuum-line. All o-ring bearing connections, PVC tubing and non-glass material were covered with aluminum foil to protect the material from the UV-light and to prevent blank carbon generation during decomposition of the material.

(2) The ultra violet light is generated by a 6 inch, 1200 Watt, medium pressure mercury arc UV-lamp by *UV Doctor*, mounted vertically on insulating ceramic stand-offs. An elliptical reflector lined with highly polished aluminum focuses the UV-light on a vertical line towards the photochemical reactor.

(3) The filled reactor is placed inside the reaction chamber on a magnetic spin plate. The chamber itself is made from lightweight steel trash cans. It is designed to provide sufficient cooling of the UV-lamp by four light reducing baffled air intakes on the base of the chamber, vent noxious gases (e.g. O<sub>3</sub>) produced during irradiation and to protect the system operator. The adjacent vacuum-line (Fig. A-4) follows the general purification and quantification procedure described above. The line is mainly manufactured from 12 mm OD standard wall

*Pyrex* tubing and sectioned by 4 mm bore all-glass high-vacuum stopcocks. Individual components are connected by spherical joints. During irradiation produced halogens are removed by bubbling through a potassium iodide solution (KI). Water and CO<sub>2</sub> are condensed in a modified Horibe-trap embedded in a dry ice/isopropanol slush [Horibe *et al.* 1973; *Beaupré et al.* 2007] and a metal ring-trap in a liquid nitrogen bath. Before quantification the CO<sub>2</sub> gas is additionally cleaned by passing through a *Pyrex* U-tube-trap embedded in dry-ice/isopropanol and finally fixated in a 16.41 mL inner volume *Pyrex* cold-finger cooled with liquid nitrogen. The cold-finger is connected to a vacuum pressure transducer (0–100 torr, *setra*) for manometric CO<sub>2</sub> quantification. Finally, the pure CO<sub>2</sub> is transferred from the cold-finger into evacuated and liquid nitrogen-cooled 6 mm glass tubes, which are then flame sealed.

### *DOC extraction procedure*

Before DOC extraction, the photochemical reactor, *Pyrex* spin bar and heat exchanger were rinsed with seralpur water and because of the small sample volume the reactor was filled with ~800 mL seralpur water. Next, the assembled reactor was placed on the magnetic spin plate within the reaction chamber. The reactor was connected with the recirculating chiller, the helium supply and to the adjacent vacuum-line and the water was pre-cleaned by UV-irradiation for 2 h.

Subsequently, the ~20 mL samples were acidified with ~1 g 85 % phosphoric acid and added to the pre-cleaned water inside the reactor, which was assembled again.

To remove all inorganic carbon from the sample the reactor was purged for ~60 min with ultra pure helium that had been scrubbed of residual CO<sub>2</sub> with Ascarite II (20 to 30 mesh, *Acros Organics*) at a flow rate of ~200 mL/min. The gas flow left the system through an outlet valve prior entering the vacuum-line.

After 60 min the helium flow was stopped, the cooler started and the vacuum-line was evacuated and carefully filled with helium to equalize the pressure in the line and the reactor. The reactor was then purged with helium for additional 15 min, but the gas now flushed through the entire vacuum-line. Due to the high flow rate and resulting overpressure, relative to the atmosphere, any residual CO<sub>2</sub> was removed from the line and any back-flush of atmospheric CO<sub>2</sub> through the gas outlet was prevented. After a total purge time of 75 min the gas outlet valve was closed, the helium flow stopped and the vacuum-line was closed behind the halogen- and water-trap and evacuated again.

Afterwards, the magnetic spin bar and the UV-light were turned on for a total UV-oxidation time of 180 min.

Thereafter, a dry ice/isopropanol slush was placed under the water-trap and a liquid nitrogen bath under the metal CO<sub>2</sub>-trap. The pressure in the vacuum-line behind the water-trap was balanced with the reactor pressure by filling with helium. To purge out all generated CO<sub>2</sub> from the reactor the irradiated sample was again purged with 150 mL/min helium for 66 min flowing through all traps to remove impurities and to collect the sample CO<sub>2</sub> in the metal CO<sub>2</sub>-trap. Halogens were removed chemically in the potassium-iodine solution, water vapor was condensed in the water-trap immersed in slush. The sample CO<sub>2</sub> was condensed in the metal CO<sub>2</sub>-trap cooled with liquid nitrogen and the helium gas escaped the vacuum-line through an outlet valve at the end. Subsequently, the individual traps were isolated from the remaining vacuum-line, which was then evacuated and the liquid nitrogen from the CO<sub>2</sub>-trap removed.

Afterwards, the sample CO<sub>2</sub> was transferred from the metal CO<sub>2</sub>-trap to the liquid nitrogen cooled cold-finger passing through a slush-cooled U-tube to remove any residual water vapor. After 4 min the cold-finger was separated from the vacuum-line and, following thermal equilibration to the ambient air temperature, the amount of CO<sub>2</sub> within the cold-finger was determined manometrically according to the ideal gas law (Eq. 4).

Finally, the pure CO<sub>2</sub> was transferred from the cold-finger to the evacuated and liquid nitrogen-cooled 6 mm glass tube which was flame sealed to collect the CO<sub>2</sub>.

### 3.2.4 Radiocarbon measurements

$^{14}\text{C}$  concentrations were determined at the NOSAMS facility at WHOI by direct counting of  $\beta$ -particles emitted during the radioactive decay of  $^{14}\text{C}$  atoms. The principles of Accelerator Mass Spectrometry (AMS) used at NOSAMS will be explained in the following based on the configuration of the 2.5 Mega electron Volt (MeV) tandem accelerator.

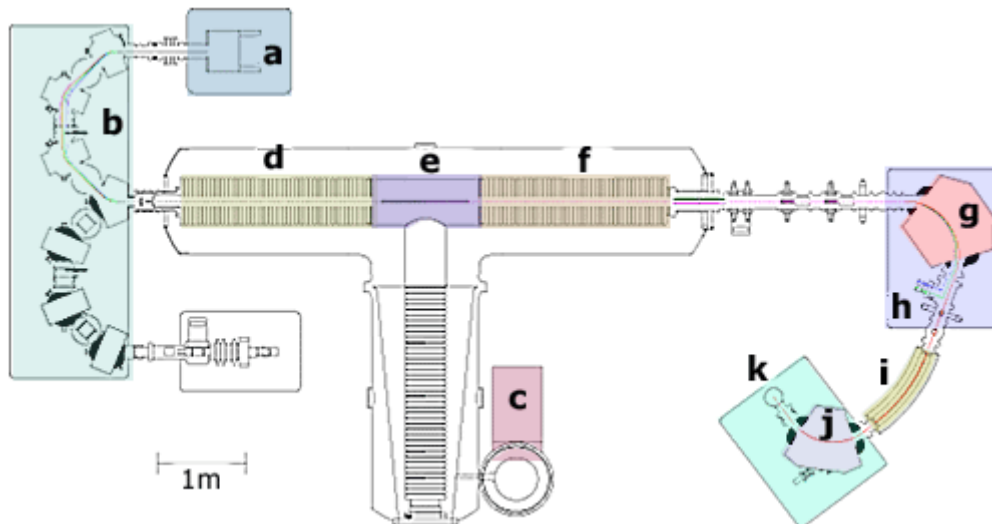


**Fig. 3: Configuration of the 2.5 MeV tandem Accelerator Mass Spectrometer at NOSAMS, WHOI.**  
a) Caesium sputter ion source; b) Recombinator injector; c) Radio-frequency power supply; d) Tandem accelerator (first stage); e) Accelerator terminal; f) Tandem accelerator (second stage); g) Main mass spectrometer; h) Two Faraday-cups; i)  $^{14}\text{C}$  analyzer; j)  $90^\circ$  bending magnet; k) Gas ionization detector (from NOSAMS [2009])

Before samples can be loaded into the AMS, the pure  $\text{CO}_2$  submitted to NOSAMS has to be converted to graphite by reduction in excess hydrogen using iron (Fe) as a catalyst. The iron-graphite mixture is then pressed into aluminum target cartridges, which are placed in a carousel and loaded into the AMS ion source (a in Fig. 3) [NOSAMS 2008].

The loaded graphite target, inside the ion source, is sputtered with heated caesium (Cs) ions producing a negative ion beam consisting of  $^{12}\text{C}^-$ ,  $^{13}\text{C}^-$  and  $^{14}\text{C}^-$  and further elemental and molecular ions. The generation of a negative ion beam is critical, since it discriminates against  $^{14}\text{N}$ , the most abundant element with the atomic mass of 14, which does not form stable negative ions. The negative ion beam is produced by a 40 kV electric field and kept in vacuum before passing through the recombinator injector (b, Fig. 3). The recombinator injector consists of four magnets and two electrostatic lenses and separates the negative ions according to their atomic masses (12, 13, and 14 amu), removes other unwanted masses and finally recombines the mostly pure negative carbon ions for the accelerator. Inside the tandem accelerator the ion beam is accelerated to  $\sim 5800$  km/sec (d, Fig 3) towards the accelerator terminal (e, Fig. 3). Within the accelerator terminal the ion beam gains a kinetic energy of 2.5 MeV and passes through an electron stripper, a canal filled with

argon (Ar) atoms. The resulting collision between ion beam and Ar atoms removes 4 valence electrons from each carbon ion and thus charge them positively ( $^{12}\text{C}^{3+}$ ,  $^{13}\text{C}^{3+}$ ,  $^{14}\text{C}^{3+}$ ) and dissociate compound ions of carbon and hydrogen ( $^{12}\text{CH}$ ,  $^{12}\text{CH}_2$ ,  $^{13}\text{CH}$ ), which are always formed during the ionization in the ion source. Emerging from the electron stripper the triple positively charged carbon ions are accelerated to  $\sim 11600$  km/sec gaining an ultimate kinetic energy of about 10 MeV (f, Fig. 3). Afterwards, the  $110^\circ$  mass spectrometer magnet bends the ion beam and separates the carbon ions based on the deflection, resulted by mass differences, into three individual beams (g, Fig. 3). The stable carbon isotope beams ( $^{12}\text{C}^{3+}$  and  $^{13}\text{C}^{3+}$ ) are collected in Faraday-cups measuring the resulting current (h, Fig. 3), whereas the  $^{14}\text{C}^{3+}$  beam passes through towards the  $^{14}\text{C}$  analyzer unit. The  $^{14}\text{C}$  analyzer unit consists of three parts, a  $33^\circ$  electrostatic deflector (i, Fig 3), removing ions with the wrong energy/charge ratio followed by a  $90^\circ$  magnet removing ions with the wrong momentum (j, Fig 3). The pure  $^{14}\text{C}^{3+}$  ions are finally collected in a gas ionization detector (k, Fig 3). The ratio of  $^{14}\text{C}$  particles per second, detected in the ionization chamber to the particle currents measured in the Faraday cups, is compared to frequently measured  $^{14}\text{C}/^{12}\text{C}$  and  $^{13}\text{C}/^{12}\text{C}$  ratios of reference standards to report final AMS  $^{14}\text{C}$  concentrations [NOSAMS 2008; Kusch 2010].

All reported  $fMC$  values are corrected for isotopic fractionation and calculated according to Eq. 1. Furthermore, they are corrected for processing blanks, the incorporated blank carbon in the AMS laboratory, and statistical uncertainty of the AMS measurement. The respective  $fMC$  error ( $\sigma fMC$ ) is calculated using the larger of either an internal statistical error (counting statistics) or an external error (reproducibility of several measurements of each sample).

### 3.3 Lena Delta

The Lena River is the second largest Arctic river in terms of discharge (averaging 581 km<sup>3</sup>/yr) and provides the Laptev Sea with 5.6–5.8 Tg DOC per year [Raymond *et al.* 2007; Holmes *et al.* 2011]. The total length of the Lena River is 4387 km and the river has its source in the mountains of the Baikal region north of Mongolia. The Lena River flows bounded by the Verkhoyansk Ridge to the east and the Central Siberian Uplands in the west northwards into the Laptev Sea through a complex braided network of channels [Zhulidov *et al.* 1997]. Its Delta is located between the Taimyr Peninsula and the New Siberian Islands. About 78–93 % of the entire Lena watershed, covering 2.46x10<sup>6</sup> km<sup>2</sup>, is underlain by permafrost with continuous permafrost extending down to 50°N [Zhang *et al.* 1999]. The northern and middle watershed parent rock material are predominantly Cambrian and Precambrian limestones, Jurassic to Cretaceous terrigenous sediments and Quaternary alluvial deposits [Rachold 1999; Amon *et al.* 2012]. The Lena Delta itself is bordered by the Chekanovsky Ridge in the southwest and the Kharaulakh Ridge in the southeast. The Delta can be subdivided into three geomorphological terraces: (i) from 1 to 12 m above sea level (masl) is a Holocene to modern currently active delta floodplain stretching along the main river channels in the central and eastern parts of the delta; (ii) fluvial Late Pleistocene sediments covering the second terrace between 20–30 masl mainly in the northwestern part (Arga Island); (iii) whereas 30–55 masl the south and southwestern area is covered by an erosional remnant of a Middle to Late Pleistocene accumulation plain. The later consists of ice-complexes including enormous layers of organic-rich material (Fig. 4) [Are & Reimnitz 2000; Schwamborn *et al.* 2002; Schirrmeister *et al.* 2011].

Samoylov Island is located in the southern central part of the river delta (72.22°N 126.30°E; Fig. 4), approximately 120 km south of the Arctic Ocean. Samoylov Island belongs to the first terrace of the Delta and is mainly dominated by Middle Holocene deposits. To the south-east the island is in contact to the main channel that drains through Holocene to modern sediments. About 10 km to the west, the channel network is in contact to a Late Pleistocene complex belonging to the third terrace of the Delta.

The climate of the southern Lena Delta is characterized by mean annual air temperatures of -14.7 °C and a mean annual precipitation of 190 mm. The winter season (end of September to end of May) is characterized by an average temperature of -30 °C, with heavy snowstorms, insufficient light (polar night) [Wagner *et al.* 2003] and low water discharge due to permanent ice coverage [Yang 2002]. The summer period is characterized by higher temperatures of about 7 °C in average, permanent light (polar day) [Wagner *et al.* 2003] and high river runoff [Yang 2002]. Maximum discharge and sediment load of the Lena within the Delta occurs generally early June due to the snowmelt flood [Yang 2002].

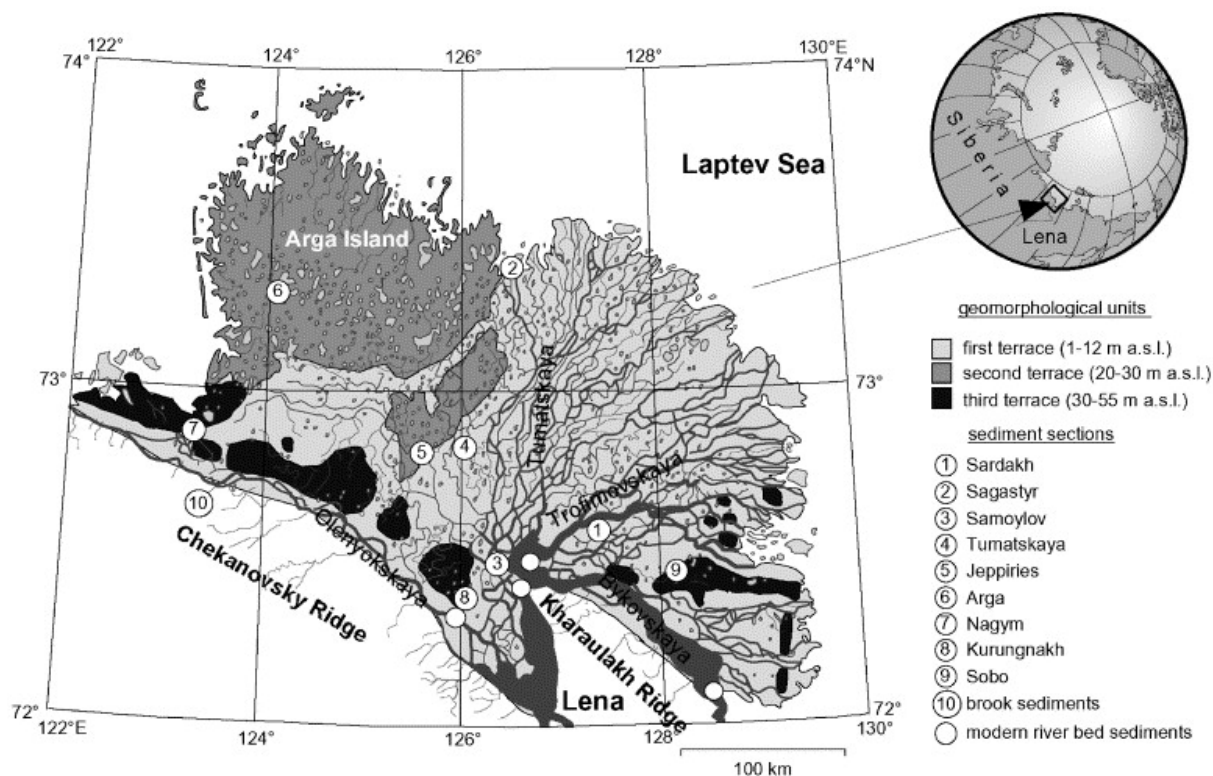


**Fig. 4: Geomorphological overview of the Lena Delta. First terrace: Holocene to modern delta floodplain (light gray); Second terrace: fluvial Late Pleistocene sediments (gray); Third terrace: erosional remnant of a Middle to Late Pleistocene accumulation plain (black). Samoylov Island is located at sample site 3. From Schwamborn *et al.* [2002].**

This work reports results for samples that have been taken during a sampling trip in summer 2011 at the AWI field camp in the south of Samoylov Island. The samples were taken within 7 days following up the main snowmelt flood (26<sup>th</sup> of June to 2<sup>nd</sup> of July) directly from the surface of the Lena near the camp station (72°22'N 126°30'E). Water samples were filtered through pre-combusted 0.45 µm glass fiber filters (*WHATMAN*). For DOC analyses the filtered water was acidified with concentrated hydrochloric acid (HCl) in the field and kept frozen as ~40 mL replicates. DOC concentrations were determined on a *Shimadzu TOC-VCPN* analyzer as described before. DO<sup>14</sup>C measurements were prepared according to the roto-evaporation (RV) procedure described above and analyzed at the NOSAMS facility, WHOI. The filters were kept frozen for supplementary analyses of the particular organic carbon (POC) performed by colleagues within the work group.

## 4. Results

### 4.1 Extraction efficiency

The amount of CO<sub>2</sub> ( $n_{CO_2}$ ) measured manometrically following the purification of the gas, was calculated according to Clapeyron's ideal gas law. The ideal gas law allows calculating the amount of gas molecules ( $n$ ) within a known volume ( $V$ ) at given temperature ( $T$ ) and pressure ( $p$ ) inside the constant volume, where  $R$  is the universal gas constant  $R = 8,31451 J/(K \times mol)$  (all results and individual variables are summarized in the appendix Tab. A-I):

$$n = \frac{p \times V}{R \times T} \quad (4)$$

The extraction efficiencies (EE) of the different methods were calculated as the amount of CO<sub>2</sub> ( $n_{CO_2}$ ) divided by the initial amount of DOC ( $n_{initDOC}$ ):

$$EE = \frac{n_{CO_2}}{n_{initDOC}} \times 100 \quad (5)$$

Tab. 2 shows the calculated extraction efficiencies for the three methods, solid phase extraction (SPE), UV-oxidation (UV) and roto-evaporation (RV), respectively. All standards and the Cow Creek samples were analyzed in duplicates for each method.

Solid phase extraction (SPE) shows minor variation of less than 5 % between duplicates for all samples. The conventional DO<sup>14</sup>C standards, oxalic acid and glycine hydrochloride, could not be extracted sufficiently with the PPL-cartridges and display average extraction efficiencies of 4 % and 13 % respectively. The resulting CO<sub>2</sub> was insufficient for <sup>14</sup>C analysis and following blank carbon determination. Therefore two more appropriate lignin phenol standards, 4-hydroxybenzaldehyde and *p*-coumaric acid, were extracted successfully. With the PPL-cartridges, 83 % of 4-hydroxybenzaldehyde and 94 % of *p*-coumaric acid on average were extracted. For the natural control Cow Creek samples, an average extraction efficiency of 78 % was achieved.

The ultraviolet-oxidation (UV) lead to average extraction efficiencies of more than 100 % for all samples, up to 116 % for glycine hydrochloride, which suggests a significant incorporation of blank carbon during sample processing. Nevertheless, the variation between duplicates is low, < 3 % for natural Cow Creek samples and glycine hydrochloride standards and < 8 % for oxalic acid.

The roto-evaporation (RV) method showed the largest variation in extraction efficiencies between duplicates of about 6 % for glycine hydrochloride, up to 12 % for oxalic acid and

14 % for the natural Cow Creek samples. The average extraction efficiency for natural Cow Creek samples and oxalic acid standards are comparable with values of 70 % and 66 %, respectively, whereas about 88 % of glycine hydrochloride was extracted.

Method	Material	$EE^1$ [%]	$fMC_{std}^2$	$fMC_{std+b}^3$	$\sigma fMC_{std+b}^3$
SPE	oxalic acid (1)	7	1.2933	n.a.	n.a.
	oxalic acid (2)	1		n.a.	n.a.
	glycine hydrochloride (1)	8	0	n.a.	n.a.
	glycine hydrochloride (2)	17		n.a.	n.a.
	4-hydroxybenzaldehyde (1)	88	0.0012	0.0543	0.0010
	4-hydroxybenzaldehyde (2)	76		0.0411	0.0012
	p-coumaric acid (1)	94	0.0101	0.0378	0.0009
	p-coumaric acid (2)	95		0.0433	0.0009
	Cow Creek (1)	77		0.8456	0.0041
	Cow Creek (2)	78		0.8098	0.0038
UV	oxalic acid (1)	114	1.2933	1.2003	0.0040
	oxalic acid (2)	99		1.2468	0.0039
	glycine hydrochloride (1)	119	0	0.0233	0.0020
	glycine hydrochloride (2)	113		0.0735	0.0021
	Cow Creek (1)	107		0.8473	0.0043
	Cow Creek (2)	104		0.8636	0.0048
RV	oxalic Acid (1)	54	1.2933	1.2878	0.0135
	oxalic Acid (2)	78		1.3217	0.0098
	glycine hydrochloride (1)	82	0	0.0518	0.0066
	glycine hydrochloride (2)	84		0.0407	0.0065
	glycine hydrochloride (3)	94		0.0247	0.0011
	glycine hydrochloride (4)	93		0.0229	0.0009
	Cow Creek (1)	56		0.8934	0.0032
	Cow Creek (2)	78		0.8942	0.0063

Tab. 2: Summary of the raw results of the method evaluation.

<sup>1</sup>Extraction efficiency calculated according to Eq. 5; <sup>2</sup>Initial, unprocessed fMC value of the standard; <sup>3</sup>processed fMC values and uncertainties reported by NOSAMS.

Key: SPE, solid phase extraction; UV, ultraviolet-oxidation; RV, roto-evaporation; n.a., not analysed.

## 4.2 $^{14}\text{C}$ analyses

The reported raw results of the  $^{14}\text{C}$  analyses of the standards and natural Cow Creek samples are summarized in Tab. 2 for every method and shown in Fig. 5 as  $fMC$  values. Fig. 5-a shows the raw  $fMC$  values of the modern oxalic acid duplicates for the roto-evaporation and UV-oxidation method. The dashed blue line indicates the true  $fMC$  value of the standard ( $fMC_{Ox} = 1.2933$ ). Measured  $fMC$  results of DOC extracted by roto-evaporation are similar to the true value (1.2878 and 1.3217) suggesting minor or isotopically similar blank carbon incorporation, whereas the results of the UV methodology differ more towards lower  $fMC$  values (1.2003 and 1.2468) indicating the incorporation of isotopically older blank carbon. The raw results for the isotopically dead standard glycine hydrochloride ( $fMC_{Gly} = 0$ ) are shown in Fig. 5-b. The  $fMC$  values of the processed standards, obtained by roto-evaporation (0.0518, 0.0409 and 0.0247) as well as UV-oxidation (0.0233 and 0.0735) are higher than the true  $fMC$  value of the standard material, suggesting the incorporation of isotopically modern blank carbon.

Since the standards, oxalic acid and glycine hydrochloride, could not be extracted sufficiently by SPE and the resulting amount of carbon was insufficient for  $^{14}\text{C}$  analyses, the results of the additionally SPE extracted isotopically old lignin phenol standards are shown in Fig. 5-c. The lignin phenol standards, 4-hydroxybenzaldehyde and *p*-coumaric acid, carry similar true  $fMC_{std}$  values ( $fMC_{4-Hydroxy} = 0.0012$  and  $fMC_{p-Coumaric} = 0.0101$ ) as indicated by dashed lines (pink for 4-hydroxybenzaldehyde and purple for *p*-coumaric acid) in Fig. 5-c. For both standards extracted by SPE, an increase in the  $fMC$  value could be observed as a result of the extraction procedure. Since the raw results of the processed standards as well as the initial true values are very similar both materials are grouped together and henceforth referred to as lignin phenol standard.

Fig. 5-d shows the raw results of the natural Cow Creek samples. Cow Creek samples were extracted and measured in duplicates for every method. The raw results vary for all three methods between  $fMC$  values of  $\sim 0.89$  for the roto-evaporation method and  $\sim 0.81$  for SPE. Basically no variation between duplicates were obtained by the roto-evaporation (0.8934 and 0.8942), small variation by UV-oxidation (0.8473 and 0.8636) and large variation between Cow Creek duplicates by solid phase extraction (0.8098 and 0.8456).

These raw results will be used in the following section to calculate the blank carbon incorporation for every method. Subsequently, the blank correction for the Cow Creek samples will be performed to further discuss the differences between the three methods.

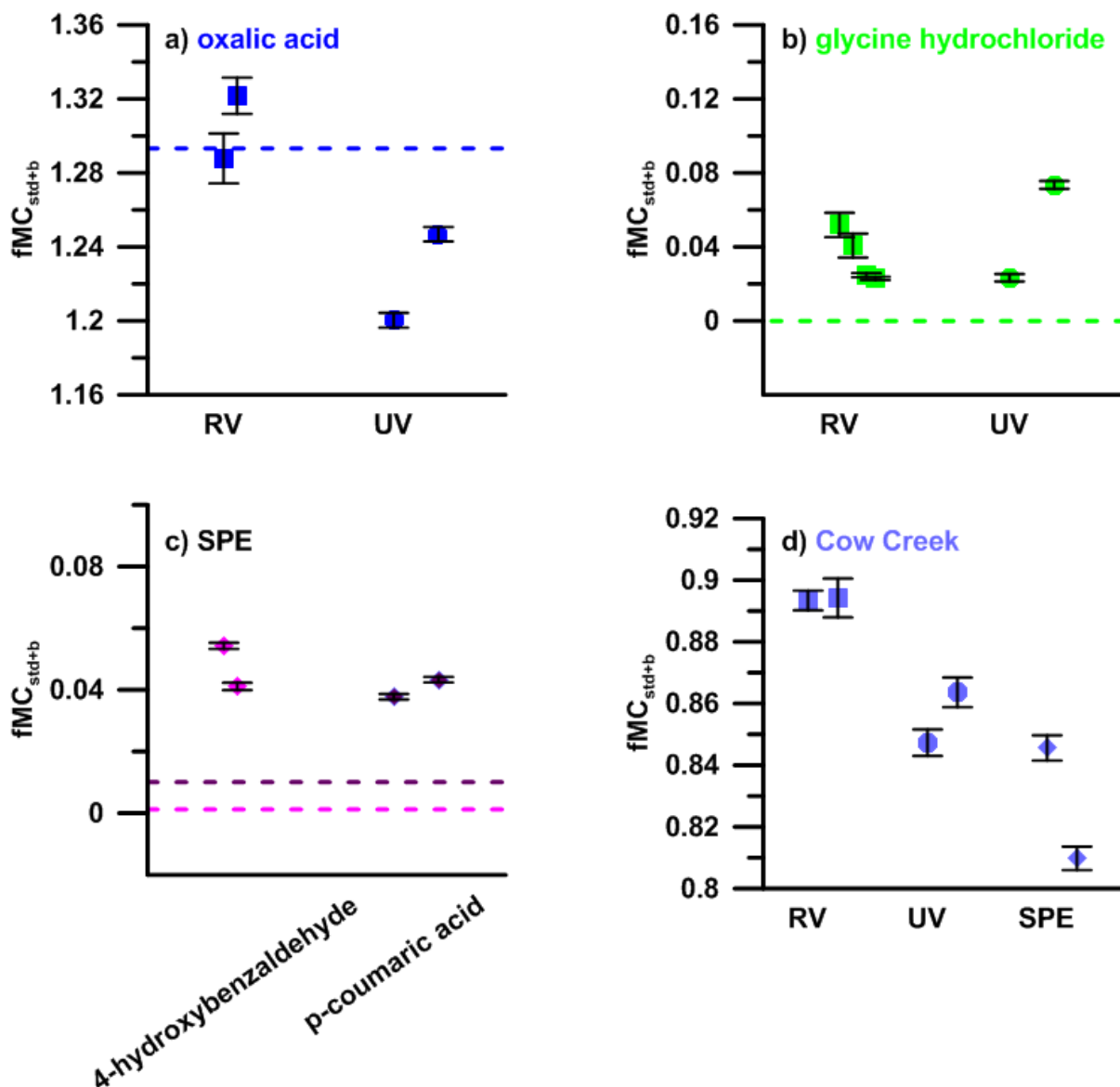


Fig. 5: Summary of reported fMC values and uncertainties of the standards and Cow Creek samples. a) Measured results of oxalic acid samples processed by RV (blue squares) and UV (blue circles), dashed blue line indicates the true fMC value of oxalic acid (1.2933); b) Measured results of glycine hydrochloride samples processed by RV (green squares) and UV (green circles), dashed green line indicates the true fMC value of glycine hydrochloride (0); c) Measured results of standards processed by SPE, 4-hydroxybenzaldehyde (pink diamonds) and *p*-coumaric acid (purple diamonds), dashed lines indicate the true fMC value of 4-hydroxybenzaldehyde (0.0012, pink) and *p*-coumaric acid (0.0101, purple); d) Measured results of Cow Creek replicates processed by RV (light blue squares), UV (light blue circles) and SPE (light blue diamonds).

Key: RV, roto-evaporation; UV, ultraviolet-oxidation; SPE, solid phase extraction.

## 4.4 Lena Delta

Sample Name	Sampling Date	DOC <sup>1</sup> [μMC]	EE <sup>2</sup> [%]	DO <sup>14</sup> C <sup>3</sup> [ <i>fMC</i> ]	<i>σfMC</i> <sup>3</sup>	DO <sup>13</sup> C <sup>3</sup> [‰VPDB]	POC <sup>4</sup> [μMC]	PO <sup>14</sup> C <sup>4</sup> [ <i>fMC</i> ]	PO <sup>13</sup> C <sup>4</sup> [‰VPDB]
L11-06	26.06.11	823	105	1.0688	0.0032	-27.8	65	0.8623	-28.3
L11-07-03	28.06.11	820	n.a.	n.a.	n.a.	n.a.	24	n.a.	n.a.
L11-08/09	29.06.11	833	88	1.0589	0.004	-27.7	56	n.a.	n.a.
L11-10/11	30.06.11	838	92	1.0703	0.0041	-27.9	85	0.8558	-29.3
L11-12/13	01.07.11	814	95	1.0613	0.0036	-27.9	64	n.a.	n.a.
L11-14/15	02.07.11	793	95	1.0701	0.0031	-28	57	0.8519	-27.7

**Tab. 3: Lena Delta sample names, sampling dates and summary of reported raw results.**

<sup>1</sup>DOC concentrations in μMC, measured at AWI Bremerhaven; <sup>2</sup>Extraction efficiency calculated according to Eq. 5; <sup>3</sup>processed *fMC* vales, corresponding uncertainties and δ<sup>13</sup>C values in ‰VPDB reported by NOSAMS; <sup>4</sup>POC concentration and stable and radiogenic isotopic composition provided by Maria Winterfeld.

The results of the Lena Delta samples collected between 26<sup>th</sup> of June 2011 and 2<sup>nd</sup> of July 2011 are summarized in Tab. 3. The DOC concentration remains stable between 790 μMC and 840 μMC within the investigated time window. Concentration increases slightly from the 26<sup>th</sup> of June reaching its maximum (838 μMC) 4 days later. From the 30<sup>th</sup> of June to 2<sup>nd</sup> of July the DOC concentration declines continuously to its minimum value (793 μMC). The sample taken at the 28<sup>th</sup> of June (L11-07-03) was lost during the <sup>14</sup>C analyses preparation and only DOC concentration could be determined. The resulting extraction efficiency of the roto-evaporation was high, between 88 and 105 % and 95 ±5% on average. The measured <sup>14</sup>C signature and simultaneously determined stable carbon (δ<sup>13</sup>C) signature of the DOC also remained stable within the 7 days. The dissolved organic carbon is modern in origin, with *fMC* values between 1.0589 and 1.0701 and uncertainties generally better than ±0.004. Its δ<sup>13</sup>C signature remained constant around -28 ‰VPDB.

## 5. Discussion

### 5.1 Introduction to blank carbon determination and correction

The measured  $fMC$  values for the standard materials differ from the commonly accepted true values. The reason for the difference is the incorporation of blank carbon during sample processing. The change in  $fMC$  of the standards for every method can be used to estimate the mass and  $fMC$  value of the blank carbon. Assuming that the incorporated blank carbon has a constant mass and  $fMC$  value in all standards processed in the same way, the reported  $fMC$  values can be blank-correct based on the blank estimations for each individual method.

The fundamental basis for the blank determination is a mass balance that can be used to calculate the true  $fMC$  values for standards using the standard dilution method [Hayes 2002; Hwang & Druffel 2005]:

$$fMC_{std+b}m_{std+b} = fMC_b m_b + fMC_{std} m_{std} = fMC_b m_b + fMC_{std} (m_{std+b} - m_b) \quad (6)$$

where  $m$  is the mass of carbon and the subscripts  $b$  and  $std$  are blank and standard, respectively. Assuming that  $fMC_b$  and  $m_b$  are constant, the mass balance (Eq. 6) can be expressed as a linear equation with  $1/m_{std+b}$  as the x-variable,  $fMC_{std+b}$  as the y-variable, the y-intercept as the true  $fMC_{std}$  value of the standard and the term  $(fMC_b - fMC_{std})m_b$  as the slope ( $M$ ) of the linear regression [Hwang & Druffel 2005]:

$$fMC_{std+b} = fMC_{std} + (fMC_b - fMC_{std})m_b \times \frac{1}{m_{std+b}} \quad (7)$$

Since the true  $fMC_{std}$  values of the unprocessed standards are known; the same approach can be used to calculate the mass and  $fMC$  value of the blank carbon when two different standards are used. If the measured  $fMC_{std+b}$  is plotted against their  $1/m_{std+b}$  value for two different standards processed in the same way, the intercept of the linear lines ( $x_0; y_0$ ) defines the  $fMC_b$  on the y-axis and  $1/m_b$  on the x-axis. Therefore, the constant terms  $fMC_b$  and  $m_b$  can be calculated for every method by a linear system of equations with two variables based on the individual slopes (Eq. 8).

$$\begin{aligned}
M_{std1} &= (fMC_b - fMC_{std1}) \times m_b \\
M_{std2} &= (fMC_b - fMC_{std2}) \times m_b
\end{aligned}
\tag{8}$$

If  $fMC_b$ ,  $m_b$  and their uncertainties can be measured directly, the blank correction of the  $fMC$  value of a sample ( $fMC_{smp}$ ) can be performed using the mass balance equation [Hwang & Druffel 2005]:

$$fMC_{smp} = \frac{fMC_{smp+b} \times m_{smp+b} - fMC_b \times m_b}{m_{smp+b} - m_b}
\tag{9}$$

Unfortunately, the mass of the blank carbon for the individual extraction methods was too small to be measured directly, but the term  $fMC_b \times m_b$  can be determined indirectly by the previously described mathematical operation. Therefore, Eq. 9 can be modified to [Hwang & Druffel 2005]:

$$fMC_{smp} = \frac{fMC_{smp+b} \times m_{smp+b} - [fMC_{std+b} \times m_{std+b} - fMC_{std} \times (m_{std+b} - m_b)]}{m_{smp+b} - m_b}
\tag{10}$$

Eq. 10 is mathematically more robust compared to Eq. 9 since for every variable the uncertainty is known or can be calculated. Thus, the total uncertainty ( $\sigma fMC_{smp}$ ) for the blank corrected  $fMC_{smp}$  can be calculated as well. The detailed equations for the total uncertainty calculation can be found in the appendix (Eq. A-I–A-IV). The blank corrected  $fMC_{smp}$  value is calculated from one sample result ( $fMC_{smp+b}$ ,  $m_{smp+b}$ ) using the results of all processed standards ( $fMC_{std+b}$ ,  $m_{std+b}$ ) for the individual extraction method. Therefore, for every measured  $fMC_{smp+b}$  value the blank correction will result in  $n$  (number of processed standards per method) different blank-corrected  $fMC_{smp}$  values. The average value of the  $n$  results of  $fMC_{smp}$  is reported as the blank-corrected  $fMC_{smp}$  value. The total uncertainty ( $\sigma fMC_{smp}$ ) is calculated using equation A-I for every blank correction and the larger value of the average of the total uncertainty ( $\sigma fMC_{smp}$ ) and the standard deviation of the  $n$  blank corrected  $fMC_{smp}$  values is reported as the final uncertainty [Hwang & Druffel 2005].

## 5.2 Blank carbon determination and correction

### 5.2.1 Ultraviolet-oxidation

The theoretically described method for the blank carbon determination and correction will be applied in detail on the example for the experimental results of the ultraviolet-oxidation method.

In Fig. 6-a and b the measured  $fMC_{smp+b}$  for the extracted glycine hydrochloride and oxalic acid standards are plotted against the manometrically determined  $1/m_{std+b}$  values. In addition, the true value  $fMC_{std}$  for the unprocessed standards, 0 and 1.2933 for glycine hydrochloride and oxalic acid, respectively, are plotted as the y-intercept. The regression lines are calculated as follows

$$fMC_{std+b} = M \times 1/m_{std+b} + fMC_{std} \quad (11)$$

with  $fMC_{std}$  as the constant for the true values of the unprocessed standards. If the regression lines are extended, their intercept values ( $x_0; y_0$  Fig. 6-c) define  $m_b$  and  $fMC_b$  of the blank.

The incorporated blank carbon during the UV-oxidation is half modern in its isotopic composition and the mass of the carbon contamination is about 8.3  $\mu\text{gC}$ . The graphic solution is not precise enough to perform a blank correction but provides quick information about the quality of the extraction method. Precise values for  $fMC_b$  and  $m_b$  can be calculated based on the two individual slopes ( $M$ ) of the regression lines:

$$\begin{aligned} M_{Gly} &= 4.61 = (fMC_b - fMC_{Gly}) \times m_b \\ M_{Ox} &= -5.61 = (fMC_b - fMC_{Ox}) \times m_b \end{aligned} \quad (11)$$

with  $fMC_{Gly} = 0$  and  $fMC_{Ox} = 1.2933$ . The linear system of equations with two variables can be solved by equalizing both equations. The calculated fraction modern carbon value of the UV-blank is  $fMC_{UV\_b} = 0.5639$  and its mass is  $m_{UV\_b} = 8.2 \pm 5.3 \mu\text{g}$ .

The precision of the calculated values is fair, since the used standards have very different  $fMC_{std}$  values and the incorporated blank carbon  $fMC_b$  value lies in between both standards. Nevertheless, a  $1\sigma$  error is applied to the calculated mass since the coefficients of regression ( $R^2$ ) with 0.63 and 0.7 for glycine hydrochloride and oxalic acid, respectively,

reveals uncertainties for the slope of the regression lines. The precision could be improved if more standards with varying masses would be extracted additionally.

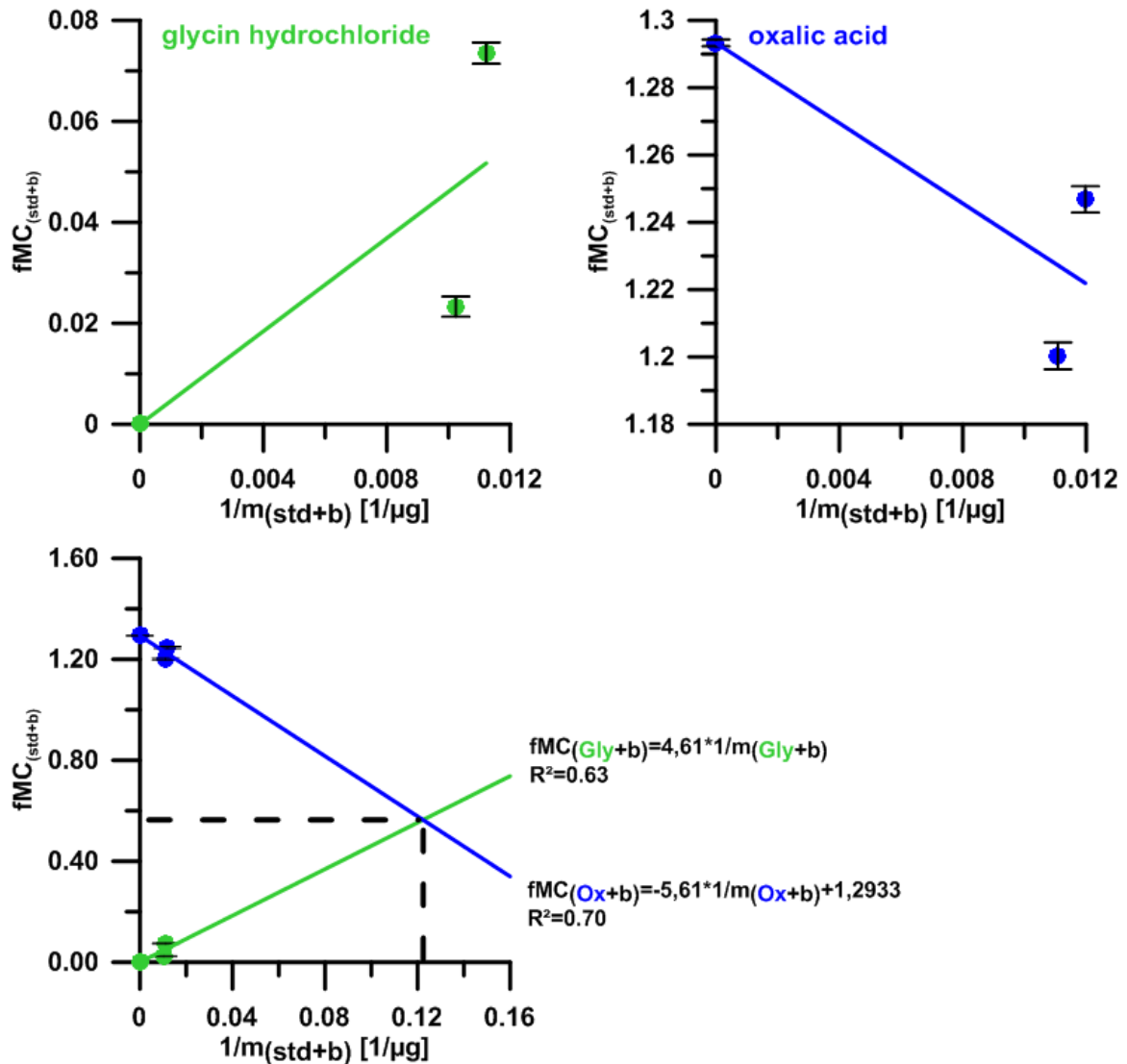


Fig. 6: Graphical illustration of the blank carbon determination for the ultraviolet-oxidation method. Upper left: fMC values vs. 1/m of processed glycine hydrochloride duplicates (green circles), trend line is calculated through the true fMC value of glycine hydrochloride (0); Upper right: fMC values vs. 1/m of processed oxalic acid duplicates (blue circles), trend line is calculated through the true fMC value of oxalic acid (1.2933); Lower left: Combination of the upper two graphs, intercept of the trend lines for glycine hydrochloride (green) and oxalic acid (blue) defines the mass ( $x_0$ ) and fMC value ( $y_0$ ) of the blank, the slopes of corresponding linear regression lines was used in Eq. 11.

### 5.2.2 Roto-evaporation

In the same way, the mass and  $fMC$  values of the blank carbon for the roto-evaporation method can be calculated (Fig 7). The RV\_blank is modern and similar in its isotopic composition to the used oxalic acid standard, causing a flat slope for the regression line and large uncertainties for the calculation of  $fMC_{RV\_b}$  and  $m_{RV\_b}$ . Hence, a  $1\sigma$  error for  $m_{RV\_b}$  was applied resulting in  $fMC_{RV\_b} = 1.5312$  and  $m_{RV\_b} = 1.9 \pm 1.2 \mu g$ . The calculated mass of carbon contamination for the roto-evaporation is much smaller than for the ultraviolet-oxidation method and, therefore, has a smaller influence of the measured  $fMC$  values of the natural Cow Creek control samples.

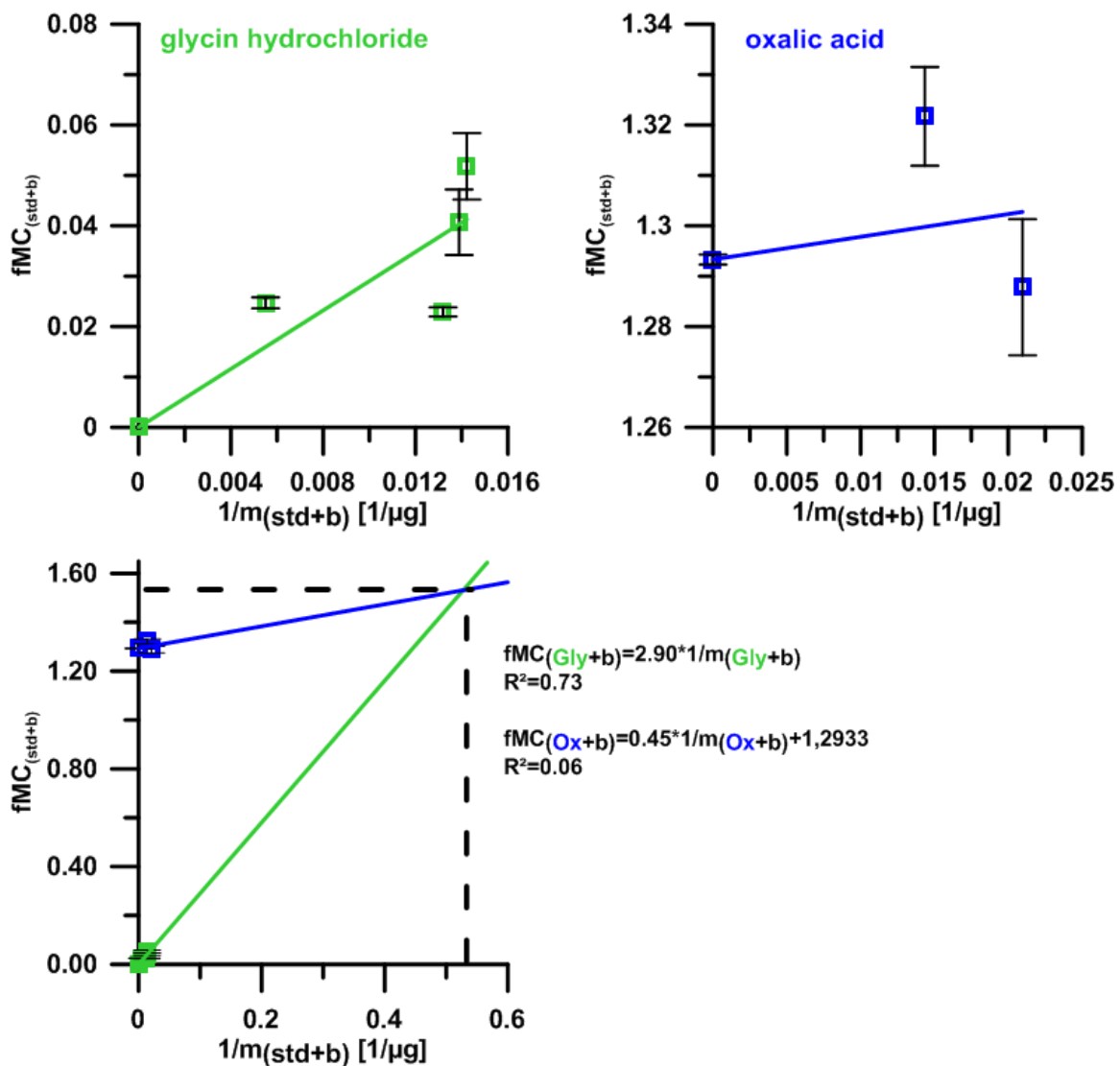


Fig. 7: Graphical illustration of the blank carbon determination for the roto-evaporation method. Upper left:  $fMC$  values vs.  $1/m$  of processed glycine hydrochloride replicates (green squares), trend line is calculated through the true  $fMC$  value of glycine hydrochloride (0); Upper right:  $fMC$  values vs.  $1/m$  of processed oxalic acid duplicates (blue squares), trend line is calculated through the true  $fMC$  value of oxalic acid (1.2933); Lower left: Combination of the upper two graphs, intercept of the trend lines for glycine hydrochloride (green) and oxalic acid (blue) defines the mass ( $x_0$ ) and  $fMC$  value ( $y_0$ ) of the blank, the slopes of corresponding linear regression line was used in Eq. 8.

### 5.2.3 Blank correction for RV and UV

With the calculated masses of the carbon contamination the measured  $fMC$  values for the natural Cow Creek samples can be blank corrected to receive better comparison of the results between the two methods. Tab. 5 shows an example of the blank correction and uncertainty determination for a measured Cow Creek sample extracted with the UV method according to Eq. 10 and Eq. A-I. Four sets of standard results ( $fMC_{std+b}$ ,  $m_{std+b}$ ) are used to correct the sample result.

The average value (0.8654) of the calculated  $fMC_{smp}$  is taken as the blank corrected true value. The larger of the average of the total calculated uncertainty ( $\sigma fMC_{smp} = 0.025$ ) and the standard deviation of the 4 blank corrected  $fMC_{smp}$  values (0.0109) is taken as the final total uncertainty. Therefore, the final blank-corrected result for the Cow Creek sample is  $fMC_{CowCreek} = 0.8654 \pm 0.025$ .

The blank corrected results for the four natural Cow Creek samples extracted by roto-evaporation and UV-oxidation are presented in Tab. 4. The outcome of the blank correction is a statistically comparable result for both extraction methods. Therefore, it is feasible to take the average value of all four blank corrected Cow Creek samples as true value with a total uncertainty following error propagation of  $fMC_{CowCreek} = 0.8736 \pm 0.0097$ .

Sample	$fMC_{smp+b}$ <sup>1</sup>	$\sigma fMC_{smp+b}$ <sup>1</sup>	$fMC_{smp}$ <sup>2</sup>	$\sigma fMC_{smp}$ <sup>3</sup>
Cow Creek RV (1)	0.8934	0.0032	0.8770	0.009
Cow Creek RV (2)	0.8942	0.0063	0.8695	0.012
Cow Creek UV (1)	0.8473	0.0043	0.8654	0.025
Cow Creek UV (2)	0.8636	0.0048	0.8827	0.025

**Tab. 4: Summary of processed and blank-corrected fMC values and uncertainties of Cow Creek replicates processed by UV and RV.**

<sup>1</sup>Processed fMC values and uncertainties reported by NOSAMS; <sup>2</sup>blank-corrected fMC values calculated according to Eq.10 and calculated total uncertainties (Eq. A-I).

Key: UV, ultraviolet-oxidation; RV, roto-evaporation.

Standard UV	$fMC_{smp+b}^1$	$\sigma fMC_{smp+b}^1$	$fMC_{std+b}^2$	$\sigma fMC_{std+b}^2$	$fMC_{std}^3$	$\sigma fMC_{std}^3$	$m_{smp+b}^4$ [ $\mu$ g]	$\sigma m_{smp+b}^5$ [ $\mu$ g]	$m_{std+b}^6$ [ $\mu$ g]	$\sigma m_{std+b}^5$ [ $\mu$ g]
oxalic acid	0.8473	0.0043	1.2003	0.0040	1.2933	0.0010	146.36	7.32	90.20	4.51
oxalic acid	0.8473	0.0043	1.2468	0.0039	1.2933	0.0010	146.36	7.32	83.50	4.18
glycine hydrochloride	0.8473	0.0043	0.0233	0.0020	0	0	146.36	7.32	97.70	4.89
glycine hydrochloride	0.8473	0.0043	0.0735	0.0021	0	0	146.36	7.32	89.10	4.46

$m_b^7$ [ $\mu$ g]	$\sigma m_b^7$ [ $\mu$ g]	$\frac{\partial fMC_{smp}}{\partial fMC_{smp+b}}$	$\frac{\partial fMC_{smp}}{\partial fMC_{std+b}}$	$\frac{\partial fMC_{smp}}{\partial fMC_{std}}$	$\frac{\partial fMC_{smp}}{\partial m_{smp+b}}$	$\frac{\partial fMC_{smp}}{\partial m_{std+b}}$	$\frac{\partial fMC_{smp}}{\partial m_b}$	$fMC_{smp}^8$	$\sigma fMC_{smp}^9$
8.17	5.25	1.0591	-0.6527	0.5936	-0.0002	0.0007	-0.0030	0.8816	0.0169
8.17	5.25	1.0591	-0.6043	0.5451	0.0000	0.0003	-0.0032	0.8490	0.0177
8.17	5.25	1.0591	-0.7070	0.6479	-0.0002	-0.0002	0.0064	0.8809	0.0338
8.17	5.25	1.0591	-0.6448	0.5856	0.0000	-0.0005	0.0062	0.8500	0.0327
								Avg= 0.8654	Avg= 0.0250
								SD= 0.0109	

Tab. 5: Example of the blank correction and total uncertainty calculation for one Cow Creek replicate processed by UV using the results of 4 processed standards. <sup>1</sup>Processed fMC value and uncertainty of the Cow Creek sample reported by NOSAMS; <sup>2</sup>Processed fMC values and uncertainties of the standards reported by NOSAMS; <sup>3</sup>True fMC values and uncertainties of the standards; <sup>4</sup>Mass of the Cow Creek replicate measured manometrically; <sup>5</sup>5% of the manometrically measured mass was assigned as uncertainty; <sup>6</sup>Mass of the standards measured manometrically; <sup>7</sup>Calculated mass of incorporated blank carbon and 1 $\sigma$  as the uncertainty; <sup>8</sup>Blank-corrected fMC values calculated according to Eq.10; <sup>9</sup>Total uncertainties of the blank-corrected fMC values, calculated according to Eq. A-I. Key: UV, ultraviolet-oxidation; Avg, average value; SD, standard deviation.

Fig. 8 shows the uncorrected  $fMC$  values for the Cow Creek samples in blue for every method and the blank corrected values in red. The RV results were corrected towards older values due to the incorporation of isotopically modern blank carbon, whereas the UV results were corrected towards isotopically modern values. The blank-corrected results vary slightly but can be grouped together. The gray box indicates the average value (dashed black line) and uncertainty of the true  $fMC_{CowCreek}$  value ( $0.8736 \pm 0.0097$ ).

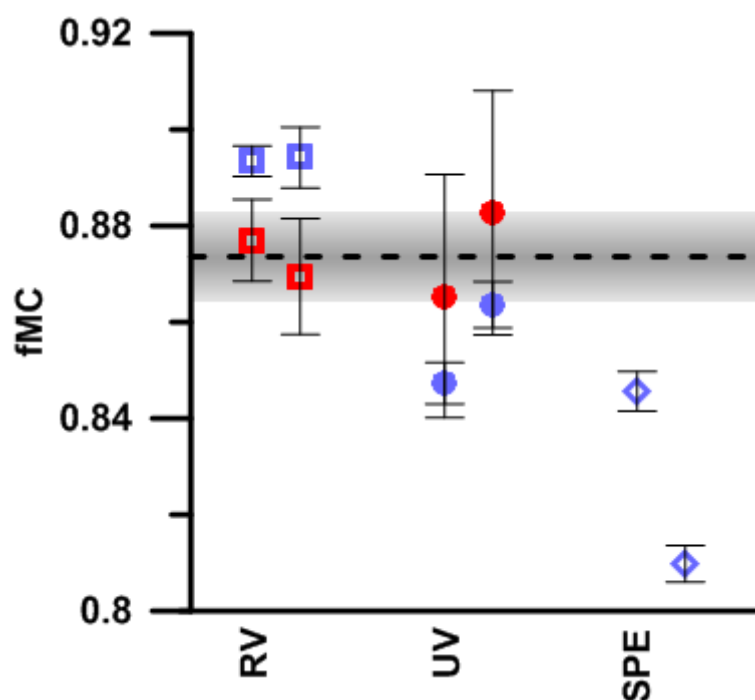


Fig. 8: Comparison between processed and blank-corrected  $fMC$  values of Cow Creek replicates. Measured  $fMC$  values processed by RV (light blue squares), UV (light blue circles) and SPE (light blue diamonds) reported by NOSAMS. Corresponding blank-corrected  $fMC$  values for RV (red squares) and UV (red circles). Dashed black line shows the true  $fMC$  value of the Cow Creek ( $0.8736 \pm 0.0097$ ) and the gray box indicates its uncertainty.

Key: RV, roto-evaporation; UV, ultraviolet-oxidation, SPE, solid phase extraction.

#### 5.2.4 Solid phase extraction

The uncorrected SPE results differ significantly from the calculated true  $fMC_{CowCreek}$  value indicating a significant blank incorporation during the solid phase extraction of DOC.

Unfortunately, the commonly used standards, oxalic acid and glycine hydrochloride, could not be extracted sufficiently and can not be used for the blank determination for the solid phase extraction method. Therefore, a set of lignin phenols (*p*-coumaric acid and 4-hydroxybenzaldehyde) was extracted and analyzed. For the blank determination, both standards can be grouped as the isotopically old lignin phenol standard. Since the unprocessed  $fMC$  values are very similar, 0.0101 and 0.0012 for 4-hydroxybenzaldehyde

and *p*-coumaric acid, respectively, the average value was used as the unprocessed real value for the lignin phenol standard ( $fMC_{Lig} = 0.0057$ ). In addition the SPE extracted and analyzed Cow Creek samples are treated as modern standard with the average blank-corrected value ( $fMC_{CowCreek} = 0.8736$ ) as true unprocessed  $fMC$  value. The blank determination was conducted as before (Fig. 9) and reveals a  $fMC$  value for the blank carbon of  $fMC_{SPE\_b} = 0.3775$  and a mass of carbon contamination of  $m_{SPE\_b} = 10.4 \pm 6.7 \mu g$  including a  $1\sigma$  error resulting from the large uncertainties as described before.

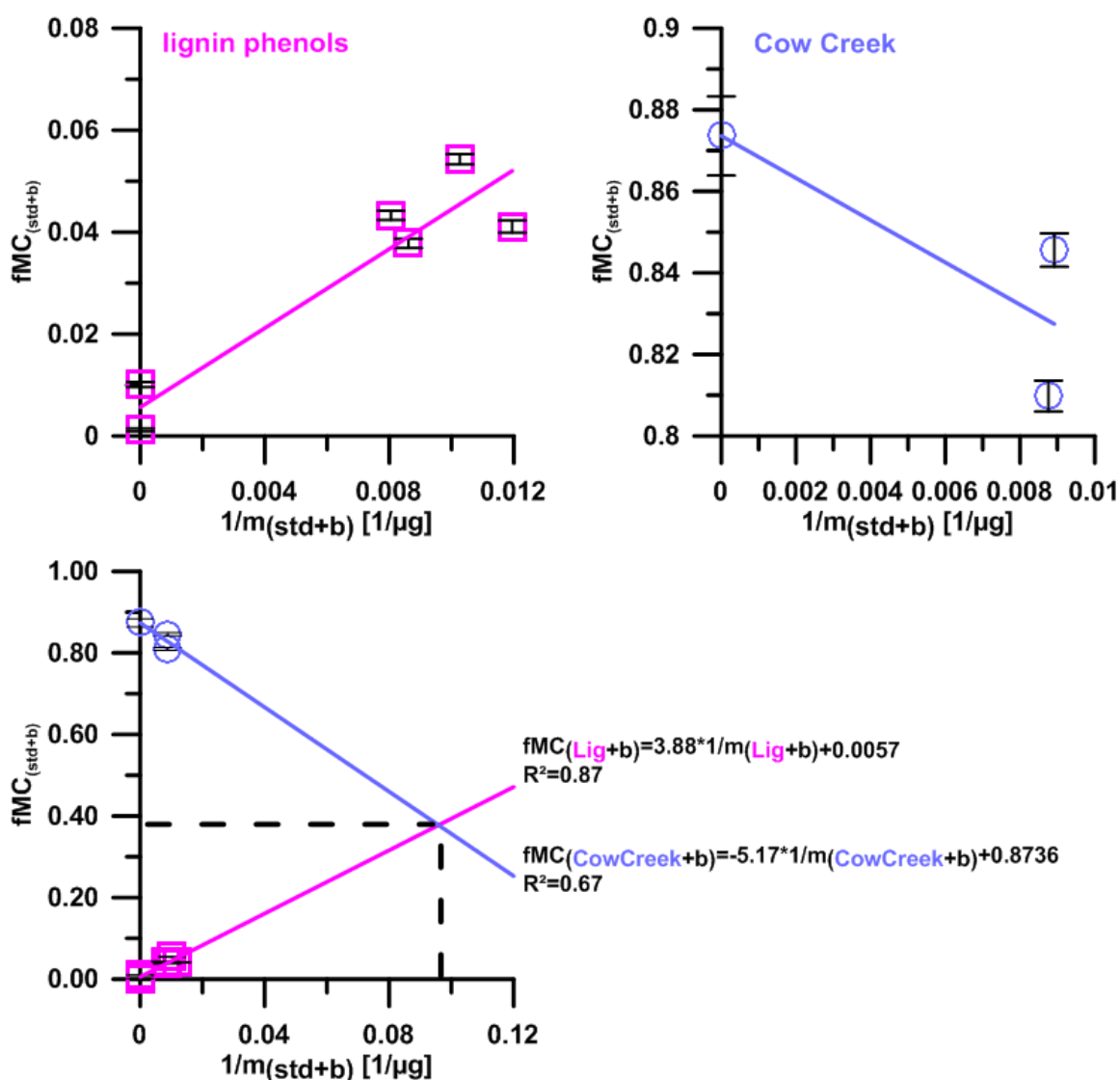


Fig. 9: Graphical illustration of the blank carbon determination for the solid phase extraction method. Upper left:  $fMC$  values vs.  $1/m$  of processed lignin phenol replicates (pink squares), trend line is calculated through the true  $fMC$  value of the lignin phenols (0.0057); Upper right:  $fMC$  values vs.  $1/m$  of processed Cow Creek duplicates (light blue circles), trend line is calculated through the true  $fMC$  value of the Cow Creek (0.8736); Lower left: Combination of the upper two graphs, intercept of the trend lines for the lignin phenols (pink) and Cow Creek (light blue) defines the mass ( $x_0$ ) and  $fMC$  value ( $y_0$ ) of the blank, the slopes of corresponding linear regression lines was used in Eq. 8.

### 5.3 Method evaluation

Method	$fMC_b$	$m_b$ [ $\mu\text{g}$ ]
roto-evaporation	1.5312	1.9 $\pm$ 1.2
UV-oxidation	0.5639	8.2 $\pm$ 5.3
solid phase extraction	0.3775	10.4 $\pm$ 6.7

**Tab. 6:** Summary of the calculated fMC value and mass of blank carbon incorporated by roto-evaporation, ultraviolet-oxidation and solid phase extraction.

The results of the blank determination for all three DOC extraction methods are displayed in Tab 6. The smallest incorporation of blank carbon was calculated for the roto-evaporation method with 1.9  $\pm$ 1.2  $\mu\text{gC}$  and is very modern in origin. The source of the contamination might be the hydrochloride acid solution used to clean the glassware, atmospheric carbon or traces of dust from the laboratory. Especially for the roto-evaporation method, the assumption that the blank is volume- and concentration-independent will be passable, if the same equipment is used, since the total amount of contamination coming from the equipment would not change for varying sample volumes or concentrations.

The total amount of incorporated blank carbon during the UV-oxidation is nearly four times higher with 8.2  $\pm$ 5.3  $\mu\text{gC}$  for  $\sim$ 800 mL pre-cleaned water and sample. For better comparison with literature values for the blank determination of the UV-oxidation system the amount of carbon contamination should be expressed as concentration. Projected to one liter of pre-cleaned water and sample, the incorporated blank carbon concentration during our set of experiments was 0.9  $\pm$ 0.6  $\mu\text{MC}$ . *Beaupré et al.* [2007] introduced the same system as low-blank oxidation system with incorporation of 0.2  $\mu\text{M}$  blank carbon. Unfortunately, it was not possible to obtain this very small blank carbon incorporation, probably as a result of the ongoing decomposition of the o-rings within the UV-reactor, due to continuous exposure to UV-light, and lack of experience in system handling. Due to the operational procedure, the sample volume ( $\sim$ 800 mL, sample plus pre-cleaned water) and irradiation time is always constant. Thus, the approach to calculate the blank carbon incorporation based on the assumption that it is volume and concentration independent is plausible, as well. It is likely that the main source of contamination is the decomposition of the o-rings. Hence, the amount of incorporated blank is rather irradiation time than volume dependent. Consequently, the amount of blank carbon will be constant for every sample that is processed with the same procedure. Nevertheless the blank should be determined for every set of experiments independently, since the blank might increase the more degraded the o-rings are.

The highest carbon contaminations were calculated for the solid phase extraction method with  $10.4 \pm 6.7 \mu\text{gC}$ . Since the cartridges had been cleaned for 24 h in methanol it is expected that all contaminations and preload of the polymer were removed. Because of that the source of the contamination is most likely the styrene divinyl benzene polymer within the cartridge used to retain the DOC during extraction or the polypropylene that the cartridge is made of. It is likely that during the exposure to water or methanol traces of the polymer or polypropylene are dissolving and remaining in the DOC extract. This indicates that the SPE blank might not be constant and volume- and concentration- independent. Especially the sample volume and accordingly, exposure time to water might increase the amount of dissolved carbon from the polymer and cartridge. For further experiments, the correlation between sample volume and blank carbon incorporation needs to be assessed, for example by extracting a set of standards with varying DOC concentrations but constant carbon amount. Nevertheless, since the volume of all extracted samples during this experiment was nearly constant ( $\sim 20 \text{ mL}$ ) a potential volume effect is negligible and the performed blank determination is reliable for this set of experiments.

The calculated and blank-corrected extraction efficiencies (amount of blank carbon subtracted from the manometrically determined amount of  $\text{CO}_2$ ) for the three methods (Fig. 10) show clear differences which will be discussed based on the chemical structures and properties of the different standard materials. The chemical structures and properties are summarized in the appendix (page A-I). The number and type of functional groups, as well as the oxygen/carbon ratio (O:C) of the individual molecules can be used to define the polarity of the standards and help in explaining differences between the three methods.

The ultraviolet-oxidation essentially converts all dissolved organic carbon into carbon dioxide as already shown by Beaupré et al. (2007). The blank corrected extraction efficiencies for oxalic acid ( $96 \pm 7 \%$ ), glycine hydrochloride ( $105 \pm 3 \%$ ) and natural Cow Creek samples ( $100 \pm 1 \%$ ) on average suggest that the UV-oxidation is not selective for certain chemical classes and that the blank-corrected  $^{14}\text{C}$  results do represent the real bulk DOC radiocarbon signature of natural samples. The calculated extraction efficiencies above 100% and variation between the duplicates are resulting from uncertainties during the manometrical determination of generated  $\text{CO}_2$

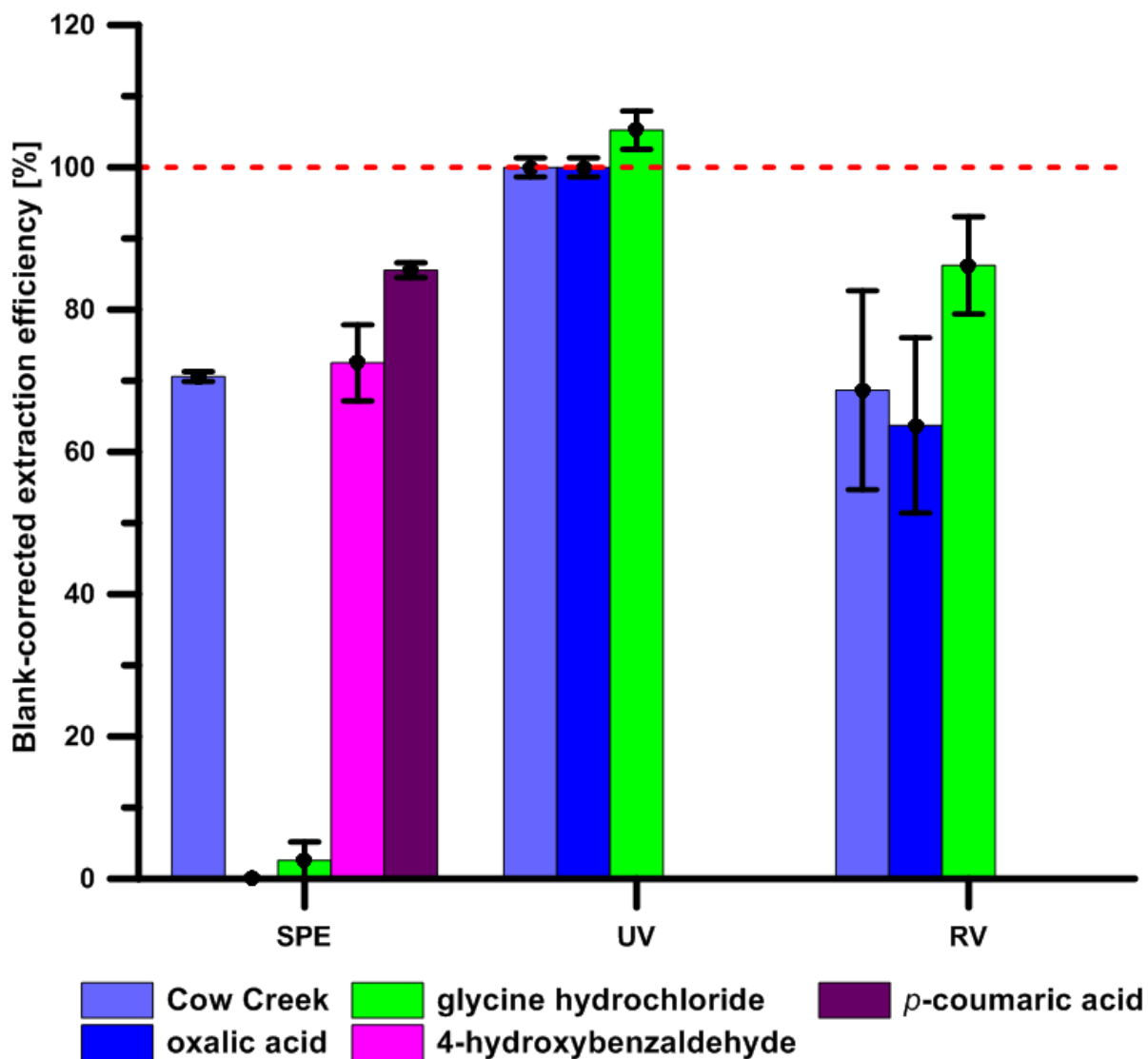


Fig. 10: Summary of blank-corrected extraction efficiencies for individual methods. Bars indicate the average values of replicates; error bars indicate variation between replicates. Blank-corrected EE are shown for Cow Creek replicates (light blue), oxalic acid (blue), glycine hydrochloride (green), 4-hydroxybenzaldehyde (pink) and *p*-coumaric acid (purple).

Key: SPE, solid phase extraction; UV, ultraviolet-oxidation; RV, roto-evaporation.

The roto-evaporation method in contrast reveals significantly lower blank corrected extraction efficiencies than the UV-oxidation. Glycine hydrochloride could be extracted most efficiently ( $86 \pm 7$  %) followed by natural Cow Creek samples ( $69 \pm 14$  %) and oxalic acid ( $64 \pm 12$  %). The greatest potentials for loss of carbon during the roto-evaporation procedure are the transfer steps during the preparation and the loss of carbon during the evaporation process itself.

The lower efficiencies and the huge variations between duplicates, up to 14 %, could be based on the methodological procedure. Deionized water was used to rinse the extracted DOC from the pear bottom flask to enable further preparation steps for the  $^{14}\text{C}$  analyses. To limit the potential of incorporation of blank carbon, only 4 mL of deionized water were used for the transfer step. Therefore, it is likely that not all extracted DOC was rinsed out. The

roto-evaporation is the most manually conducted method and thus carries the highest probability of operator-induced variations between samples. Taking into account that thereby the extraction efficiency of the comparable standards (e.g. similar polarity) glycine hydrochloride and oxalic acid is most likely depending on the accuracy of the manual transfer steps, the variation between duplicates and different standards is negligible.

On the other hand, during the evaporation of the water, following the principles of a distillation of a solution containing various components, components within the solution with the lowest boiling points will be removed from the water first. This does not impact the extraction efficiency of the standards, since their boiling points are higher than water, but it does affect natural samples. For example, during the distillation of a natural sample at ambient pressure, all components dissolved in the water with a boiling point lower than 100 °C will be removed prior to the water. By decreasing the pressure (in this experiment 70 mbar) the boiling point of water was lowered to ~50 °C but it also affected all other components. Dissolved components in natural waters with boiling points below 100 °C at ambient pressure are short chain alkanes, alcohols and non-polar low-molecular-weight components (LMW). During the roto-evaporation these components are removed from the bulk DOC and might change the measured <sup>14</sup>C signature of the sample.

For example, in arctic permafrost regions, especially in northeastern Siberia, very high methane fluxes from tundra soils were observed, leading to a high methane load of the adjacent rivers [Tsuyuzaki *et al.* 2001; van Huissteden 2005]. The amount of methane released from arctic soils is believed to depend on the thickness of the active layer, the watershed and moreover, on the type of vegetation and microbial activity [Tsuyuzaki *et al.* 2001; Wagner *et al.* 2003; van Huissteden 2005; Wille *et al.* 2008]. Methane produced by microbial methanogenesis from substrates available in the active layer of the soils would therefore reflect the <sup>14</sup>C signature of the source organic matter. It would not vary significantly from the bulk DO<sup>14</sup>C transported by the river draining, for example, Holocene formations. Nevertheless, ongoing global warming and permafrost thawing lead to an exposure of methane originating from deeper and older geologic formations. As shown by Zimov *et al.* [1997] and summarized by Walter *et al.* [2006] methane bubbles from Siberian thaw lakes are released from Pleistocene formations underneath the lake due to the ongoing warming and thawing of the permafrost. Since the methane released from Pleistocene formations can be older than the organic matter within the active layer of near surface soils, the microbial incorporation of this old carbon would alter the <sup>14</sup>C signature of the transported DOC. Unfortunately, due to the removal of methane and associated LMW during the roto-evaporation of natural samples, crucial information about the origin of the methane is lost and the true bulk DO<sup>14</sup>C signature may be skewed towards more modern-appearing values.

This concerns particularly the calculation of carbon fluxes to adjust the global carbon cycle and to distinguish between old and fresh methane.

Although one can assume that the roto-evaporation influences the measured  $^{14}\text{C}$  signature of a sample by removing dissolved methane or LMW for instance, no effect could be observed for the analysed and blank-corrected natural Cow Creek samples. The blank-corrected  $f\text{MC}$  values of the samples prepared by roto-evaporation are very similar to those extracted by ultraviolet-oxidation. Assuming that ultraviolet-oxidation is non selective and does represent the real bulk  $\text{DO}^{14}\text{C}$  signature the removal of methane and LMW by roto-evaporation might be negligible for natural samples from temperate climate zones due to the lower methane concentrations in the water and the presumably homogenous origin of the DOC. With the present dataset it is not possible to predict how the removal of methane and LMW by RV influences the  $\text{DO}^{14}\text{C}$  values of natural samples. Hence, it becomes crucial to perform addition comparison experiments between RV and UV with natural samples for each environment of interest to determine the quality and accuracy of the reported  $f\text{MC}$  values.

In comparison, the solid phase extraction with PPL-cartridges discriminates against short-chain and highly polar components, which is indicated by the low extraction efficiency for oxalic acid (0 %) and glycine hydrochloride ( $3 \pm 3$  %). Thereby, less polar and larger molecules, like the lignin phenols *p*-coumaric acid and 4-hydroxybenzaldehyde, were extracted sufficiently with  $86 \pm 1$  % and  $73 \pm 5$  %, respectively.

The higher extraction efficiency for glycine hydrochloride compared to oxalic acid supports the findings of *Dittmar et al.* [2008] that PPL-cartridges are useful to extract and analyze dissolved organic nitrogen (DON). The results show that for similar sized molecules the functional groups, and therefore polarity, defines the extraction efficiency of PPL-cartridges. Amino functional groups are less polar and better retained by the polymer than hydroxyl groups with respect to small and highly polar components like oxalic acid ( $\text{C}_2\text{H}_2\text{O}_4$ ; two hydroxyl groups;  $\text{O}:\text{C}=2$ ) and glycine hydrochloride ( $\text{C}_2\text{H}_6\text{NO}_2 \cdot \text{HCl}$ ; one amino and one hydroxyl group;  $\text{O}:\text{C}=1$ ). For larger molecules the extraction efficiency becomes higher the less polar the molecule is. The influence of functional groups on the polarity of a molecule is decreasing with increasing length of the hydrophobic carbon chain. For example the extraction efficiency of 4-hydroxybenzaldehyde ( $\text{C}_7\text{H}_6\text{O}_3$ ; two hydroxyl groups;  $\text{O}:\text{C}=0.43$ ) is  $\sim 13$  % lower than that of *p*-coumaric acid ( $\text{C}_9\text{H}_8\text{O}_3$ ; two hydroxyl groups;  $\text{O}:\text{C}=0.33$ ). The chemical structure of both molecules is similar except that *p*-coumaric acid consists of two more carbon atoms lowering the polarity and increasing the carbon density of the molecule, which leads to better adsorption on the polymer within the cartridge.

These findings are important to consider once interpreting natural SPE-DOM data. The discrimination against short-chain and polar components will likely result in the partly or complete loss of the bioactive fraction of DOM in natural waters. The bioactive fraction of

DOM contains carbohydrates such as mono- and disaccharides, short-chain organic acids and neutrals, as shown by incubation experiments of fractionized DOC samples from arctic permafrost thaw leachates and river samples [Hurst *et al.* 1985; Malcolm & MacCarthy 1992; Michaelson & Ping 1998]. For example glucose (C<sub>6</sub>H<sub>12</sub>O<sub>6</sub>; five hydroxyl groups; O:C=1), the most present monosaccharide and important substrate for microbes, is highly polar and, therefore, most likely not or only partly retained by the PPL-polymer. These observations may become even more important when working with radiocarbon data, where the analyzed <sup>14</sup>C signature is believed to reflect the bulk age of the DOC, but the discrimination against the bioactive and modern fraction of DOC would cause a shift towards older <sup>14</sup>C signatures and not reflecting the bulk DOC signature.

The extraction efficiency for the natural Cow Creek samples with 70 ± 1 % is similar to previously reported extraction efficiencies for river and tributary DOC samples (62 ± 6 %) for the same method [Dittmar *et al.* 2008]. The loss of ~30 % carbon during the extraction of natural samples supports the previous findings that certain chemical classes are not retained by the PPL-polymer. Since the Cow Creek samples had to be treated as a standard to calculate the blank carbon incorporation for the SPE method, important information about the potential loss of certain DOC fractions are lost. Nevertheless, the average raw and not blank corrected *fMC* values for Cow Creek samples extracted by the PPL-cartridges are lower (0.8277) compared to the average raw results for samples extracted by roto-evaporation (0.8938) and UV-oxidation (0.8555). The lower *fMC* value might indicate a partly loss of the isotopically modern bioactive fraction of the natural DOC, but it could also be a result of the incorporation of isotopically old blank carbon. Hence, it is not possible to further differentiate the source of the slight offset. A set of isotopically modern standards should be extracted and used for the blank carbon determination instead of the Cow Creek samples. The use of appropriate standards is essential to determine the effect of the removal of the bioactive fraction on the reported *fMC* values for natural samples. In addition comparative tests between the methods for every environment of interest seem to be crucial to evaluate the quality of the finally reported data.

## 5.3 Lena Delta

### 5.3.1 Blank correction and data reliability

Tab. 3 summarizes the results of the Lena Delta samples. The very low blank carbon incorporation of the roto-evaporation method (1.9  $\mu\text{gC}$ ) and large sample sizes of the Lena Delta samples ( $\sim 270$   $\mu\text{gC}$  on average) resulted in minor changes in  $fMC$  values ( $<1$  %) and a small decrease in the average extraction efficiency (1 %) after blank-correction. This supports the applicability of roto-evaporation for  $\text{DO}^{14}\text{C}$  preparation when sample sizes are much larger than the expected blank the blank-correction becomes insignificant.

Surprisingly, the average blank-corrected extraction efficiency of the Lena Delta samples is with  $94 \pm 6$  % very high compared to the Cow Creek samples ( $69 \pm 14$  %). Under the assumption that the low extraction efficiency results primarily from the loss of non-polar low-molecular-weight components during the roto-evaporation process, the high EE for the Lena Delta samples suggests that only minor traces of LMW were dissolved in the water. In addition, the high EE shows that no method specific fractionation of the DOC occurred and paired with the blank correction the reported  $\text{DO}^{14}\text{C}$  data reflects the bulk  $\text{DO}^{14}\text{C}$  signal and no further corrections are necessary.

### 5.3.2 Origin of organic matter in the Lena Delta

Measured DOC and POC concentrations as well as their  $fMC$  values are shown in Fig. 11. DOC and POC concentrations and  $fMC$  values behave similar within the investigated week and remain fairly stable. DOC is  $^{14}\text{C}$ -enriched and  $\sim 10$ -times more abundant compared to POC. The variation in the  $^{14}\text{C}$  signature indicates that the organic matter in both fractions originates from different sources.

The dissolved organic carbon samples are enriched in  $^{14}\text{C}$ , compared to POC. The isotopically modern average  $fMC$  value of 1.061 reveals that the carbon was fixed during the past 50 years. The younger age of the DOC compared to POC can be explained by their different forms of weathering and transport. Whereas POC enters a river predominantly by physical weathering of adjacent soils, DOC export from soils mainly occurs during surficial chemical weathering [Raymond & Bauer 2001a]. Near-surface chemical weathering includes leaching of litter and below surface production. Additionally, the DOC can be derived from riverine primary production.

The Lena Delta is predominated by wet- and dry-land grasses as well as mosses [Schneider *et al.* 2009] with typical C3-plant  $\delta^{13}\text{C}$  signatures ranging between  $-25$  to  $-30$  ‰VPDB [Pancost & Boot 2004]. Unfortunately as shown by Lobbes & Fitznar [2000] the  $\delta^{13}\text{C}$  signature of algal-derived DOC in Russian rivers falls in a similar range ( $-23.5$  to  $-29$  ‰VPDB) as the

autochthonous material derived from litter leaching. Because of that a separation between primary production introduced and autochthonous DOC is not feasible. The measured stable carbon signature of the DOC in the Delta ( $\delta^{13}\text{C} = -28\text{‰VPDB}$ ), therefore, only confirms that it is a mixture of organic material originating from surficial litter leaching and primary production within the water column.

The particular organic carbon is  $^{14}\text{C}$ -depleted with respect to current atmospheric  $^{14}\text{CO}_2$ . The average *fMC* value (0.8567) of the presented POC samples reveals a conventional radiocarbon age of >1200 years. Deltas represent highly active riverine regimes with massive accumulations of sediments and continuously ongoing erosion of adjacent soil horizons. Due to the flat terrain, the low current velocity of the water is mainly causing lateral erosion along the riverbanks. Therefore it is likely that most of the POC originates from the mechanical weathering of young surface-near Holocene soils present around the Delta. Nevertheless, possible minor contribution of older POC originating from the erosion of the Pleistocene formation to the west of the sample site cannot be excluded. The average  $\delta^{13}\text{C}$  signature of the POC (-28.7 ‰VPDB) supports the finding that the POC derives from the erosion of young soils evolved under modern days like vegetation. POC also derives from primary production within the river, but similar to DOC a differentiation of both sources is not feasible due to the overlapping  $^{13}\text{C}$  signatures of autochthonous and primary production derived organic material. Nevertheless, detailed compound specific radiocarbon dating may provide valuable insights into the small-scale contribution to POC.

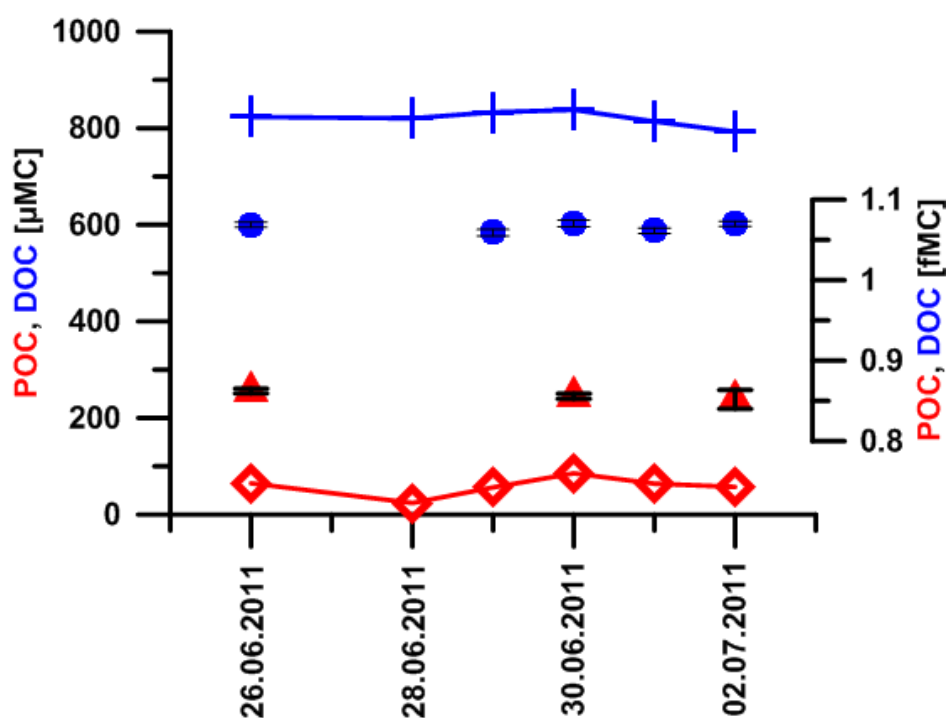


Fig. 11: Summary of POC and DOC concentrations and radiogenic carbon composition for investigated Lena Delta (at Samoylov) samples. DOC (blue crosses) and POC (red diamonds) concentration in  $\mu\text{MC}$ ;  $\text{DO}^{14}\text{C}$  (blue circles) and  $\text{PO}^{14}\text{C}$  (red triangles) composition in *fMC*.

### 5.3.3 Fate of DOC along the Lena River

It has been shown that annual constituent fluxes, as well as water discharge varied in between 1999 and 2003 from year to year [Holmes *et al.* 2011]. Nevertheless, seasonal trends on this short time frame remain fairly stable. Due to the lack of available data, annual variability will not be considered in the following and only seasonal changes will be discussed. For comparison of the Lena Delta sample with additional Lena River data, generated over the last couple of years, the year of sample collection is neglected and only the day in the year is considered. Additional Lena River DOC data has been generated by the *PARTNERS* project and is available, without restriction, through the *Arctic-GRO* data portal ([www.arcticgreativers.org](http://www.arcticgreativers.org)).

The sample site of the *PARTNERS* project (Zhigansk; 66°46'N 132°22'E) is approximately 900 km upstream from Samoylov Island. Comparing both data sets, therefore, provides information about the fate of organic matter during its transport along the river.

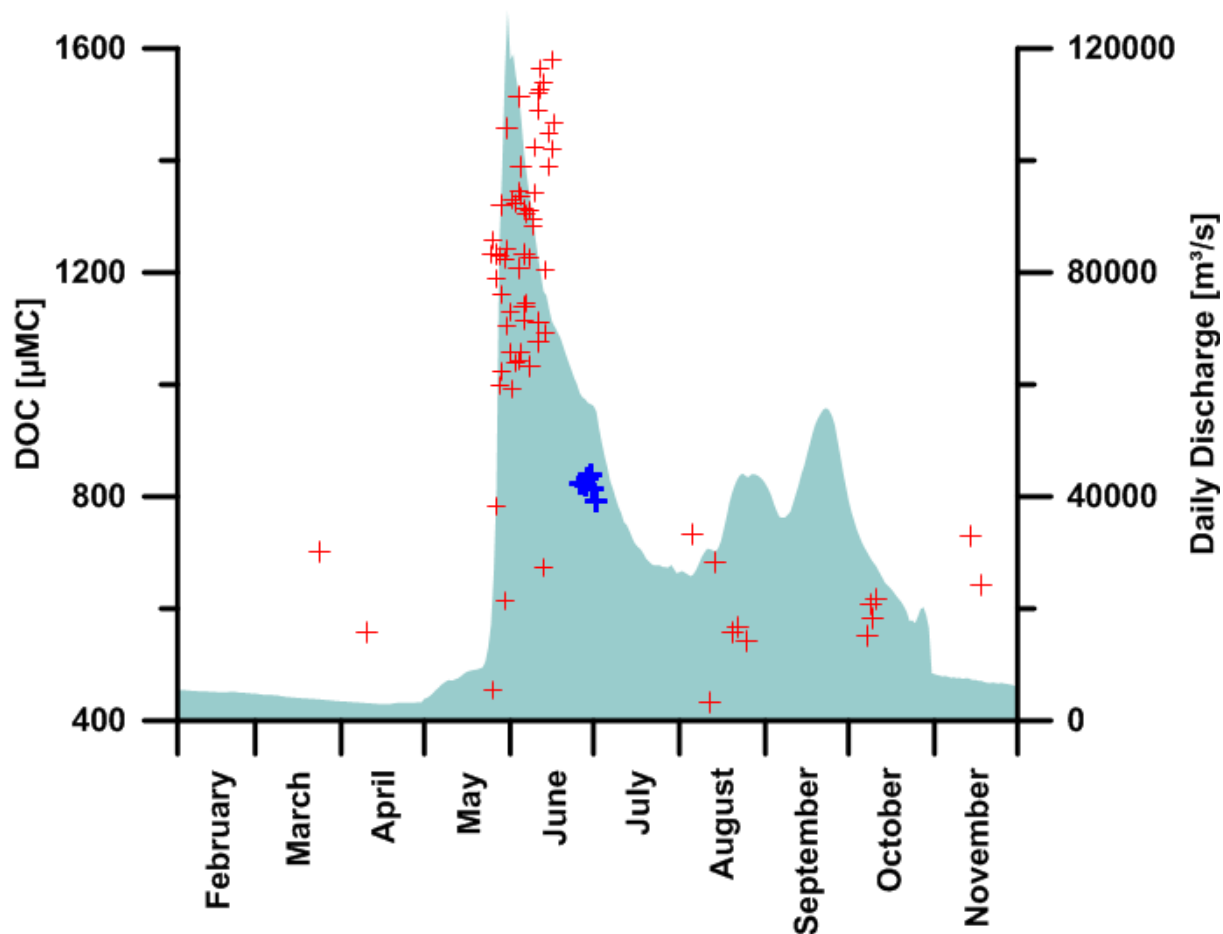


Fig. 12: Comparison of Lena River (at Zhigansk) and Lena Delta (at Samoylov) DOC concentrations between February and November in relation to Lena River discharge. Lena Delta DOC concentration (blue crosses); Lena River DOC concentration (red crosses), provided by the *PARTNERS* project ([www.arcticgreativers.org](http://www.arcticgreativers.org)); Daily water discharge (light blue background) at Kusur available through the *ArcticRIMS* data portal ([www.rims.unh.edu](http://www.rims.unh.edu)).

Fig. 12 shows the DOC concentration measured at Zhigansk between 2003 and 2011 for the day of the year (red crosses), as well as Lena Delta DOC concentrations determined in this study (blue crosses). Daily water discharge (light blue background) is reported for 2008 at the gauging station Kusus (70.68°N 127.39°E) approximately 180 km upstream from Samoylov Island. Data is available through the *ArcticRIMS* data portal ([www.rims.unh.edu](http://www.rims.unh.edu)) provided by the *University of New Hampshire Water Systems Analysis Group*.

No clear correlation between DOC concentration and water discharge can be observed. Nevertheless, highest DOC concentrations were measured during the daily water discharge maximum between end of May and early June. The high water discharge is in conjunction with the onset of the snowmelt typically occurring at the end of May [Yang 2002]. The high DOC concentrations reveal from the increase of chemical surface weathering during the snowmelt. The light offset between DOC concentration maximum in Zhigansk (end of June) and water discharge maximum further north (early June) might reveal from annual variation in the onset of the snow melt. The majority (~70 %) of DOC concentrations were measured for 2009 and 2010, but so far no water discharge data is available for these years. Nevertheless, elevated DOC concentrations can be observed for nearly the entire June. The broader extend of elevated DOC concentration in the south compared to water discharge in the north additionally shows that DOC concentrations in the river are not only triggered by the snowmelt. It is likely that DOC concentration remain high after the snow melt due to increased chemical weathering of freshly exposed soils, for example, by rain fall. Meteoric water will not affect the total discharge as much as the water introduced by melting snow, but also lead to elevated DOC concentrations in the south.

However, DOC concentrations in the Lena Delta seem to follow the water discharge trend. Highest DOC concentrations could be expected during the main snowmelt flood in early June and declining concentrations following the decrease in water discharge. Unfortunately, no data was generated during the main flood, but the measured, slightly elevated, DOC concentration at the end of June/early July supports the assumption that DOC concentrations are mainly triggered by the snowmelt along the Delta.

Nevertheless, the DOC concentrations near Samoylov are smaller than one would assume. DOC is transported in dissolved aqueous form and therefore its residence time should equal that of the water [Raymond & Bauer 2001a]. Given a mean flow propagation speed of 88 km/day [Smith & Pavelsky 2008] and an estimated flow distance between Zhigansk and Samoylov of 900 km one could expect that elevated DOC concentrations near Zhigansk should be measured within the Delta approximately 10–11 days later. Nevertheless, a continuous propagation of the elevated DOC concentration front towards the Delta could not be observed. Highest DOC concentrations (~1500 µMC) at Zhigansk were measured around the 12<sup>th</sup> of June 2010 whereas two weeks later in 2011 the concentration at Samoylov was

around 800  $\mu\text{M}$ C. Although annual variations between the sample years might partially explain the offset, it is more likely that the majority of the DOC present near Zhigansk does not reach the Delta or Arctic Ocean. Without being able to further clarify the sink for DOC during its transport along the Lena, it is likely that the DOC is being consumed by microbes, degraded by photo-oxidation or removed from the water by flocculation [Raymond & Bauer 2001b] en route.

These findings imply that the DOC in the Lena Delta predominantly originates from local vegetation, soils and primary production. The carbon isotopic signature of the DOC supports this idea. While  $\text{DO}^{13}\text{C}$  is similar on average in Zhigansk (-27 ‰VPDB) and the Delta (-28 ‰VPDB),  $\text{DO}^{14}\text{C}$  reveals minor differences in the age of the organic matter. The similar  $\delta^{13}\text{C}$  signature can be explained by similar sources of the DOC. It is likely that the algal derived DOC has a similar isotopic composition in the south and the north. In addition, Zhigansk still belongs to the permafrost region with typical C3-plant dominated tundra vegetation and Holocene soils comparable to the Delta. The terrestrial export of DOC around Zhigansk therefore has a similar stable carbon isotopic signature to that in the Delta.

Fig. 13 shows the  $^{14}\text{C}$  signature of the DOC from Zhigansk (red crosses) and the Delta (blue crosses) for the time following the snow melt. The DOC near Zhigansk becomes progressively older after the snowmelt, indicating that the process of DOC generation transits from the surface into deeper soil levels [Neff *et al.* 2006]. If the DOC in the Lena would mainly be the same as the DOC in Zhigansk, one would assume that the  $^{14}\text{C}$  signature of DOC in the Delta follows the depletion trend of the River DOC near Zhigansk and plots on or near the regression line. However, this correlation could not be observed, thereby confirming that the DOC from Zhigansk is removed and DOC in the Delta originates predominantly from local sources.

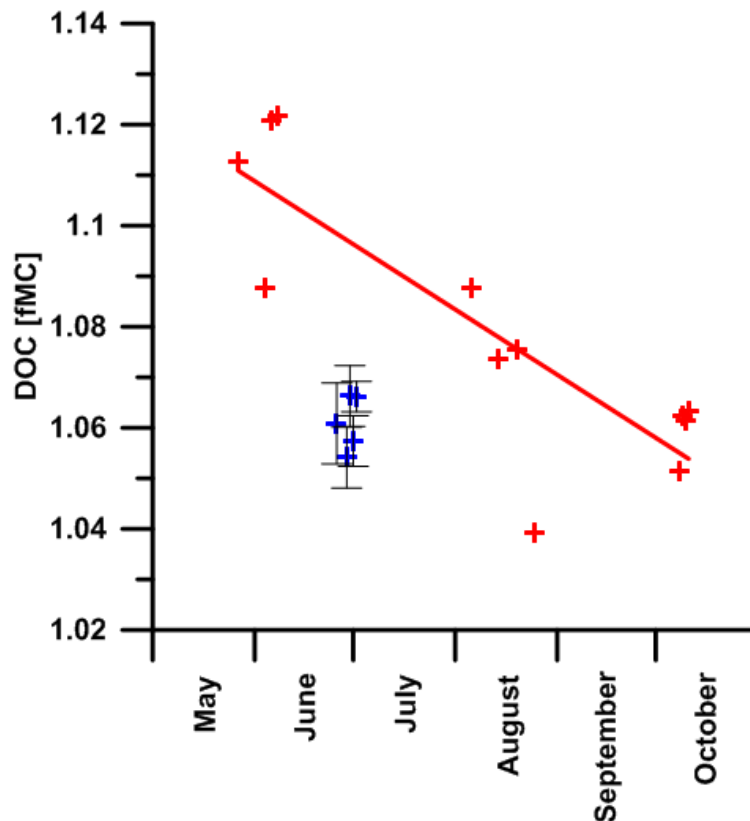


Fig. 13: Comparison of Lena River (at Zhigansk) and Lena Delta (at Samoylov)  $\text{DO}^{14}\text{C}$  composition between May and October. Lena Delta  $\text{DO}^{14}\text{C}$  composition (blue crosses); Lena River  $\text{DO}^{14}\text{C}$  composition (red crosses), provided by the *PARTNERS* project ([www.arcticgreatrivers.org](http://www.arcticgreatrivers.org)). Regression line indicates continuous  $\text{DO}^{14}\text{C}$  depletion for the Lena River (red line) during the late season.

#### 5.3.4 Arctic river DOC and thawing permafrost

As the climate, vegetation cover and seasonal cycles of northern latitudes change into the future, as a result of the global climate change, DOC fluxes will likely change as well [Neff *et al.* 2006]. Whereas, the majority of DOC fluxes will be mostly affected by changes in the brief period of late spring peaks in DOC concentration and water flux, changes in the late season DOC fluxes from Arctic rivers may be the first indication for terrestrial response to the global warming [Neff *et al.* 2006].

Neff *et al.* [2006] presented results for the Kolyma River, east Siberia, that indicate a progressive  $^{14}\text{C}$  depletion for dissolved organic carbon during the late season. Paired with lignin biomarker composition, they postulated that during the main flood riverine DOC predominantly originates from litterfall leaching, whereas towards the later season the DOC generation transits towards deeper soils. In permafrost regions, DOC generation is limited due to the thickness of the active layer overlaying the frozen soil; the deeper the thawing of the permafrost the larger becomes the active layer. In a conventional geologic setting, youngest material at the surface, the organic matter becomes progressively older with increasing depth below the surface. Since DOC generation is limited to the active layer, the

DO<sup>14</sup>C signature, therefore, provides an integrated age signal of the active layer. Hence, the terrestrial export DOC becomes older, the broader the active layer becomes. Since extend of the active layer is defined by the thawing depth of the permafrost, the DO<sup>14</sup>C signature, thus, provides information about permafrost thawing dynamics. The reported presents of older carbon in the DOC fraction of the Kolyma by *Neff et al.* [2006], therefore, provides the first indications of enhanced permafrost thawing and remobilization of previously stabilized carbon. However, due to the lack of available data, they were not able to investigate whether or not the observed late season signal is specific to the Kolyma watershed, related to ongoing regional warming, or can be observed in other Arctic rivers as well.

Fig. 14 summarizes <sup>14</sup>C signatures of DOC transported during the late season in the Lena River and Delta (north-east Siberia), Kolyma River (east Siberia) and the Mackenzie River (north Canada). The Lena Delta (blue crosses) data was generated during this work. Lena River (red crosses) and Mackenzie River (black circles) data are provided by the *PARTNERS* project and the Kolyma River (green circles) data was reported by *Neff et al.* [2006].

The Kolyma River DOC shows a clear <sup>14</sup>C depletion during the late season as described by *Neff et al.* [2006]. The depletion is illustrated by a linear regression line (green). The Lena River DOC shows <sup>14</sup>C depletion as well. However, the slope of the regression line is flatter compared to the depletion trend of the Kolyma River DOC. Although, the DOC from the Lena River and Kolyma River have similar <sup>14</sup>C signatures at the end of the snowmelt (early June), the DOC in the Kolyma River ages more significantly during the late season.

Whereas, towards the end of the year Kolyma River DOC reveals conventional radiocarbon ages of >500 yrs, Lena River DOC remains isotopically modern. Under the assumption of a conventional geologic setting and comparable soil formation processes along the Lena and Kolyma River this indicates varying permafrost thawing dynamics along both rivers. As previously described, the presents of fossil carbon can indicate the remobilization of stabilized carbon by permafrost thawing. The increased ageing of DOC in the Kolyma compared to the Lena River, therefore, indicates enhanced and deeper permafrost thawing in the east of Siberia than in the north-east.

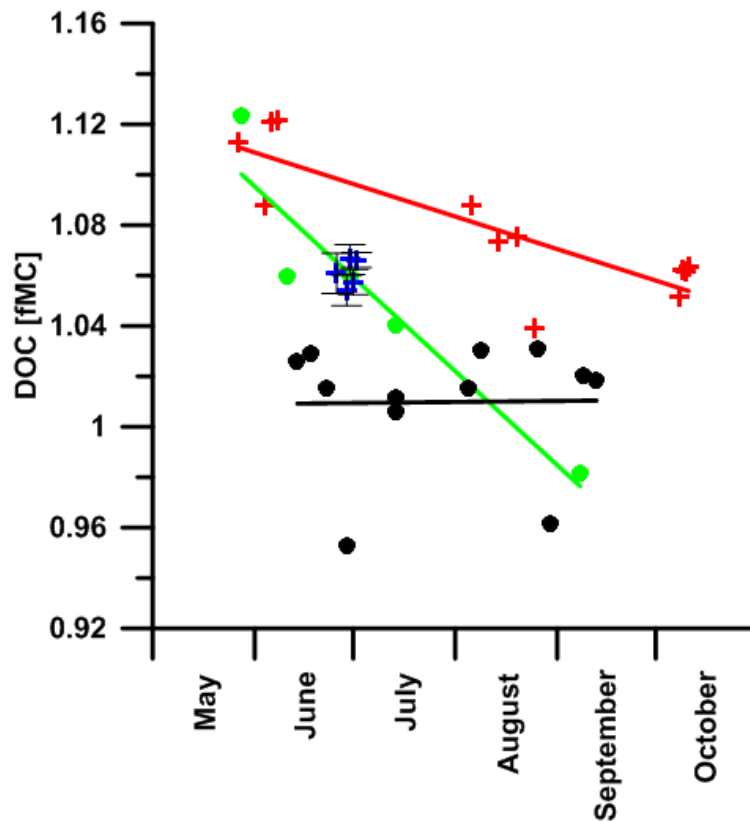


Fig. 14: Comparison of Lena River (at Zhigansk), Lena Delta (at Samoylov), Kolyma River (at Cherskii) and Mackenzie River (at Tsiigehtchic)  $\text{DO}^{14}\text{C}$  composition between May and October. Lena Delta  $\text{DO}^{14}\text{C}$  composition (blue crosses); Lena River (red crosses) and Mackenzie River (black circles)  $\text{DO}^{14}\text{C}$  compositions, provided by the *PARTNERS* project ([www.arcticgreatrivers.org](http://www.arcticgreatrivers.org)); Kolyma River (green circles)  $\text{DO}^{14}\text{C}$  composition from *Neff et al.* [2006]. Regression lines indicate continuous  $\text{DO}^{14}\text{C}$  depletion for Lena River (red line) and Kolyma River (green line), but no depletion for the Mackenzie River (black line) during the late season.

However, the DOC signature in the Lena Delta does not fit to the depletion trend observed for Lena River DOC, but rather follows the depletion trend of the Kolyma River. As described above, the majority of DOC present in the Lena Delta derives from local sources, either terrestrial or from primary production. Again, under the assumption of a conventional geologic setting and comparable soil formation this indicates that extent and depth of permafrost thawing in the Lena Delta is similar to the Kolyma River region. The geographic positions of sampling sites, for all three systems, reveal further insights into this observation. Lena River samples were taken near Zhigansk ( $66^{\circ}46'\text{N}$   $132^{\circ}22'\text{E}$ ), Delta samples on Samoylov ( $72^{\circ}22'\text{N}$   $126^{\circ}30'\text{E}$ ) and Kolyma River samples close to the shore near Cherskii ( $68^{\circ}50'\text{N}$   $161^{\circ}50'\text{E}$ ). Under the assumption, that permafrost thawing dynamics behave similar in the Lena Delta and Kolyma River regime, the geographic positions suggest that thawing dynamics are closely correlating with latitude and, thus, distance to the Arctic Ocean. The Lena Delta and Kolyma river sample sites are both further north and closer to the Arctic Ocean than the Lena River sample site and are, therefore, more vulnerable for climatic changes along the Arctic Ocean. Although, Zhigansk is located only  $\sim 4^{\circ}$  further south than

the Delta, it is likely that the Delta region and the Siberian Arctic Ocean shore regions respond quicker and comparable to climatic changes than the Siberian hinterland.

However, no such observation could be made for the Mackenzie River in north Canada. The Mackenzie River sampling site is located near Tsiigehtchic (67°30'N 133°50'W), approximately 200 km south of the shore line, therefore, one would expect to observe a  $\text{DO}^{14}\text{C}$  depletion trend similar to those observed for near shore Siberian rivers. The Mackenzie River DOC, however, shows no  $^{14}\text{C}$  depletion during the late season (Fig. 14). The constant  $^{14}\text{C}$  signature suggests that no previously stabilized carbon is remobilized due to enhanced permafrost thawing in north Canada. It remains unclear why North American coastal permafrost dynamics differ from Siberian permafrost dynamics.

The annual mean air and sea surface temperature increase during global warming is predicted to be the highest for the Arctic Ocean during the next century [IPCC 2007]. However, the coastal-near release of old and previously stabilized carbon during the late season may prove the already ongoing climate change in the northern latitudes. It remains unclear why north Siberian permafrost responses, or responses faster to the ongoing climate change than North American permafrost. It might indicate that Siberian permafrost is, somehow, more vulnerable to climatic changes in the Arctic Ocean and will experience the most dramatic changes associated to global warming.

## 6. Conclusion

Over the last couple of years, riverine DOC became an intensified field of research. Various methods have been used to extract DOC from the aqueous phase for radiocarbon analyses by different authors. However it has never been proven that the generated data is inter-methodologically comparable. This thesis provides valuable insights into the data comparability, blank carbon incorporation, constraints and limitations for roto-evaporation, UV-oxidation and solid phase extraction methods.

Under the assumption that the blank carbon incorporation for each method is constant, thus sample volume and DOC concentration independent, the amount of blank carbon can be calculated following the sample dilution procedure introduced by *Hwang & Druffel* [2005].

The ultraviolet oxidation procedure introduced by *Beaupré et al.* [2007] incorporates  $8.2 \pm 5.3 \mu\text{gC}$  and has been shown to be non selective for certain chemical classes. The UV-oxidation method therefore provides the most reliable bulk  $\text{DO}^{14}\text{C}$  data for riverine samples.

The experiments reveal smallest blank carbon incorporation for the roto-evaporation DOC extraction method ( $1.9 \pm 1.2 \mu\text{gC}$ ). The methodological procedure however provides the possibility of the loss of non-polar low-molecular-weight components (LMW) during the DOC extraction. The calculated DOC extraction efficiency for Cow Creek samples show a loss of ~25 % carbon during the extraction, however the blank corrected  $\text{DO}^{14}\text{C}$  signature is similar to the bulk  $\text{DO}^{14}\text{C}$  signature received by UV-oxidation. This suggest that the loss of LMW does not alter the  $^{14}\text{C}$  signature. Data obtained by roto-evaporation provides reliable bulk  $\text{DO}^{14}\text{C}$  results for samples from temperate climate zones due to the homogeneity of the organic matter. The extraction efficiency for the Lena Delta samples was much higher (~95 %) suggesting the absence of LMW. The bulk  $^{14}\text{C}$  signature is therefore not altered by the loss of LMW and the roto-evaporation method provides reliable  $\text{DO}^{14}\text{C}$  results. However, it remains unclear whether or not the observed effects of the roto-evaporation are exemplary for the investigated climatic regimes. For further clarification additional experiments are mandatory to define the reliability of riverine  $\text{DO}^{14}\text{C}$  data from different climatic regimes. However, the presented results show that the roto-evaporation is a solid and inexpensive alternative to the UV-oxidation to obtain riverine DOC data from arctic and temperate climatic regimes.

The solid phase extraction with PPL-cartridges showed the highest incorporation of blank carbon ( $10.4 \pm 6.7 \mu\text{gC}$ ). The blank carbon probably originates from the dissolution of the absorber polymer in sample water or MeOH necessary to elute the sorbent. However this could not be proven, it is likely that the incorporation of blank carbon is not sample volume independent and might increase with increasing sample amount. Additional experiments are necessary to clarify the dependency of blank carbon incorporation on sample volume. In

addition the SPE clearly discriminates against polar short-chain components. Polar short-chain components like carbohydrates are important substrates and by-products of biological activity and therefore an important part of the bioactive fraction of DOC [Hurst *et al.* 1985; Malcolm & MacCarthy 1992; Michaelson & Ping 1998]. The loss of the predominantly isotopically modern bioactive fraction of the DOC by solid phase extraction will cause a shift towards older  $^{14}\text{C}$  signatures and not reflecting the bulk  $\text{DO}^{14}\text{C}$  composition. In summary, due to the remaining uncertainties about blank carbon incorporation and the removal of the bioactive fraction of DOC, SPE might not be an appropriate method to extract riverine DOC.

For the second part of this thesis a set of water samples from the Lena Delta (northeast Siberia) were extracted by roto-evaporation and their DOC concentration as well as stable and radiogenic carbon isotopy determined. Samples were collected shortly after the snowmelt introduced flood at the end of June and early July 2011.

Stable and radiogenic signatures reveal that the DOC in the Delta is isotopically modern and originates from litter leaching and surface near weathering of Holocene soils. POC is isotopically older and less abundant than DOC and originates from the erosion of predominantly Holocene riverbanks. However, incorporation of terrigenous export carbon from close by Pleistocene formations can not be excluded. Additional experiments, like the investigation of Pleistocene soil pore water biomarker composition or bulk POC and DOC  $^{13}\text{C}$  and  $^{14}\text{C}$  signatures, are necessary to define the proportion of terrigenous export carbon from Pleistocene formations to the bulk organic matter in the Delta. Detailed investigations on small-scale carbon cycling within the Delta are complicated due to the lack of data and available sample material. Investigating the carbon cycling within the Delta becomes more important as it was shown that the DOC within the Delta predominantly originates from the Delta region itself. The discrepancy between DOC concentrations 900 km upstream and the Delta as well as the  $\text{DO}^{14}\text{C}$  signatures suggest that a major portion of the DOC is removed from the water en route either by microbes, photo oxidation or flocculation. This implies that the majority of terrigenous export carbon to the Arctic Ocean originates from coastal-near regions and for the implications to the global carbon cycle it becomes more important to understand coastal-near small-scale carbon dynamics rather than hinterland dynamics.

The over regional response of coastal-near regions to ongoing climate warming could be shown by comparing  $\text{DO}^{14}\text{C}$  depletion trends during the late season. Whereas the DOC becomes just slightly older during the later season 900 km upstream of the Delta, the  $\text{DO}^{14}\text{C}$  signature within the Delta seem to follow the strong  $\text{DO}^{14}\text{C}$  depletion trend of the Kolyma River [Neff *et al.* 2006]. The release of old and previously stabilized carbon in coastal-near regions results from the progressive thawing of permafrost in response to warming of the Arctic Ocean. The warming affects coastal-near region stronger than the hinterland.

However, no such observation could be made for costal-near permafrost in north Canada. The Mackenzie River shows no  $\text{DO}^{14}\text{C}$  depletion during the late season, suggesting that the predicted global warming will affect the permafrost and climate in Siberia stronger than North America.

## 7. Acknowledgments

I would like to thank **Gesine Mollenhauer** for giving me the opportunity to experience the world of radiocarbon science, enabling my research stay at **WHOI** and all her support during the working process, but especially for the marvellous time in her working group.

**Gesine**, thank you for nearly 5 years of remarkable mentoring, all the enabled chances and everything you taught me.

Additionally, I would like to thank **Boris Koch** for his friendly and helpful supervision. **Claudia Burau** for her great introduction into DOC sample handling and the SPE method, as well as the support during the concentration measurements at the **AWI** in Bremerhaven.

I also want to express my thanks to **Ann McNichol** for giving me the opportunity to use the UV system at **NOSAMS** and to **Li Xu** for his great introduction into the system (and the rides to the grocery store). Additionally, I would like to thank the entire **NOSAMS** staff for the fast processing of my samples.

Furthermore, I am grateful to **Helene Hoffmann** and the entire **GLACIOLOGY WORKING GROUP** at the **IUP** for the spontaneous access to their vacuum-line system when I was in desperate need of it.

Special thanks to **Maria Winterfeld**, **Katja Hockun** and **Andreas Basse** for the fun-time in the office, the many coffee, ice and b... breaks and their support and encouragement during long-lasting vacuum-line sessions. As well as to **Ralph Kreutz** and **Jens Hefter** for their great technical support.

I am deeply grateful for the support of my family. **Gudrun** and **Bruno** without you covering my back none of this would be possible.

And finally I want to thank my friends **Christian Hallmann**, **Colin McGovern** and **Thomas Evans** for proof-reading, valuable inputs and long-lasting discussions. But most of all I want to thank you and **all my friends** for the fun-time beside work.

You made the last 5 years  
legendary

## 8. References

- Amon, R.M.W. et al. 2012. "Dissolved organic matter sources in large Arctic rivers." *Geochimica et Cosmochimica Acta* 94:217–237.
- Are, F, and Erk Reimnitz. 2000. "An overview of the Lena River Delta setting: geology, tectonics, geomorphology, and hydrology." *Journal of Coastal Research* 16(4):1083–1093.
- Bauer, J.E., P.M. Williams, and E.R.M. Druffel. 1992. "14C activity of dissolved organic carbon fractions in the north-central Pacific and Sargasso Sea." *Nature*.
- Beaupré, S.R., E.R.M. Druffel, and Sheila Griffin. 2007. "A low-blank photochemical extraction system for concentration and isotopic analyses of marine dissolved organic carbon." *Limnology and Oceanography: Methods* 5:174–184.
- Damon, P.E., J.C. Lerman, and A. Long. 1978. "Temporal fluctuations of atmospheric 14C: causal factors and implications." *Annual Review of Earth and Planetary Sciences* 6.
- Dittmar, Thorsten, Boris Koch, Norbert Hertkorn, and Gerhard Kattner. 2008. "A simple and efficient method for the solid-phase extraction of dissolved organic matter (SPE-DOM) from seawater." *Limnol. Oceanogr. Methods* 6:230–235.
- Field, CB, and MR Raupach. 2004. *The Global Carbon Cycle: Integrating Humans, Climate, and the Natural World*. Washington (DC): Island Press.
- Flerus, R. et al. 2011. "A molecular perspective on the ageing of marine dissolved organic matter." *Biogeosciences Discussions* 8(6):11453–11488.
- Friedlingstein, P et al. 2006. "Climate–Carbon Cycle Feedback Analysis: Results from the C4MIP Model Intercomparison." *Journal of Climate* 19(14):3337–3353.
- Giorgi, Filippo, PH Whetton, and RG Jones. 2001. "Emerging patterns of simulated regional climatic changes for the 21st century due to anthropogenic forcing." *Geophysical research* 28(17):3317–3320.
- Hayes, John M. 2002. "Practice and Principles of Isotopic Measurements in Organic Geochemistry."
- Hedges, John I. 1992. "Global biogeochemical cycles: progress and problems." *Marine Chemistry* 39(1-3):67–93.
- Holmes, Robert Max et al. 2011. "Seasonal and Annual Fluxes of Nutrients and Organic Matter from Large Rivers to the Arctic Ocean and Surrounding Seas." *Estuaries and Coasts* 35(2):369–382.
- Horibe, Yoshio, Koji Shigehara, and Yasue Takakuwa. 1973. "Isotope separation factor of carbon dioxide- water system and isotopic composition of atmospheric oxygen." *Journal of Geophysical Research* 78(15).
- van Huissteden, J. 2005. "High methane flux from an arctic floodplain (Indigirka lowlands, eastern Siberia)." *Journal of Geophysical Research* 110(G2).

- Hurst, J. L., G. J. F. Pugh, and D. W. H. Walton. 1985. "The effects of freeze-thaw cycles and leaching on the loss of soluble carbohydrates from leaf material of two subantarctic plants." *Polar Biology* 4(1):27–31.
- Hwang, J, and E.R.M. Druffel. 2005. "Blank correction for d14C measurements in organic compound classes of oceanic particulate matter." *Radiocarbon* 47(1):75–87.
- IPCC. 2007. *Climate Change 2007 : An Assessment of the Intergovernmental Panel on Climate Change*.
- Jorgenson, MT, CH Racine, and JC Walters. 2001. "Permafrost Degradation and Ecological Changes Associated with a Warming Climate in Central Alaska." *Climatic Change* 551–579.
- Karlén, I, I.U. Olsson, P Kallberg, and S Kilicci. 1968. "Absolute determination of the activity of two C-14 dating standards." *Arkiv Geofysik*.
- Koch, B, K Ludwichowski, G Kattner, T Dittmar, and M Witt. 2008. "Advanced characterization of marine dissolved organic matter by combining reversed-phase liquid chromatography and FT-ICR-MS." *Marine Chemistry* 111(3-4):233–241.
- Koch, B, M Witt, R Engbrodt, T Dittmar, and G Kattner. 2005. "Molecular formulae of marine and terrigenous dissolved organic matter detected by electrospray ionization Fourier transform ion cyclotron resonance mass spectrometry." *Geochimica et Cosmochimica Acta* 69(13):3299–3308.
- Kusch, Stephanie. 2010. "Tracing time in the ocean: Unraveling depositional and preservational timescales using compound-specific radiocarbon analysis of biomarkers from marine sediments." *Fachbereich Geowissenschaften der Universität Bremen*.
- Lobbes, JM, HP Fitznar, and G Kattner. 2000. "Biogeochemical characteristics of dissolved and particulate organic matter in Russian rivers entering the Arctic Ocean." *Geochimica et Cosmochimica Acta* 64(17):2973–2983.
- Malcolm, RL, and P MacCarthy. 1992. "Quantitative evaluation of XAD-8 and XAD-4 resins used in tandem for removing organic solutes from water." *Environment International* 18:597–607.
- Mann, WB. 1983. "An international reference material for radiocarbon dating." *Radiocarbon* 25(2):519–527.
- Meybeck, Michel. 1982. "Carbon, nitrogen, and phosphorus transport by world rivers." *American Journal of Science* 282(40).
- Michaelson, GJ, and CL Ping. 1998. "The character and bioactivity of dissolved at thaw and in the spring runoff Waters of the arctic tundra north slope, Alaska." *Journal of geophysical research*.
- NOSAMS. 2008. *General Statement of 14C Procedures at the National Ocean Sciences AMS Facility*. Retrieved (<http://www.who.edu/fileserver.do?id=62825&pt=2&p=74887>).
- NOSAMS. 2009. "NOSAMS tandetron AMS system." Retrieved ([http://www.who.edu/cms/images/ams2\\_109772.gif](http://www.who.edu/cms/images/ams2_109772.gif)).

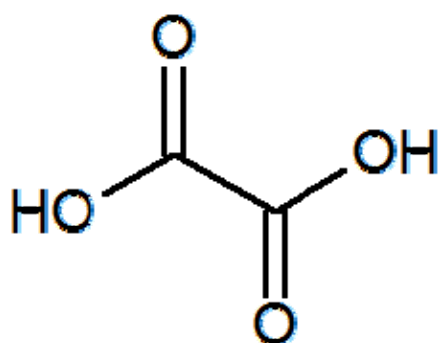
- Neff, J. C. et al. 2006. "Seasonal changes in the age and structure of dissolved organic carbon in Siberian rivers and streams." *Geophysical Research Letters* 33(23):1–5.
- Pancost, R D, and C S Boot. 2004. "The palaeoclimatic utility of terrestrial biomarkers in marine sediments." *Marine Chemistry* 92(1-4).
- Peterson, Bruce J et al. 2002. "Increasing river discharge to the Arctic Ocean." *Science (New York, N.Y.)* 298(5601):2171–3.
- Peterson, Michael L, Susan Q Lang, Anthony K Aufdenkampe, and John I Hedges. 2003. "Dissolved organic carbon measurement using a modified high-temperature combustion analyzer." *Marine Chemistry* 81(1-2):89–104.
- Rachold, V. 1999. "Major, trace, and rare earth element geochemistry of suspended particulate material of East Siberian rivers draining to the Arctic Ocean." in *Land-ocean systems in the Siberian Arctic: Dynamics and history*, edited by H. Kassens et al. Springer Berlin.
- Raymond, P.A., and J.E. Bauer. 2001a. "Use of <sup>14</sup>C and <sup>13</sup>C natural abundances for evaluating riverine, estuarine, and coastal DOC and POC sources and cycling: a review and synthesis." *Organic Geochemistry* 32(4):469–485.
- Raymond, PA, and J E Bauer. 2001b. "DOC cycling in a temperate estuary: a mass balance approach using natural <sup>14</sup>C and <sup>13</sup>C isotopes." *Limnology and Oceanography* 46(3):655–667.
- Raymond, Peter a. et al. 2007. "Flux and age of dissolved organic carbon exported to the Arctic Ocean: A carbon isotopic study of the five largest arctic rivers." *Global Biogeochemical Cycles* 21(4):1–9.
- Schirrmeister, Lutz et al. 2011. "Late Quaternary paleoenvironmental records from the western Lena Delta, Arctic Siberia." *Palaeogeography, Palaeoclimatology, Palaeoecology* 299(1-2):175–196.
- Schmidt, Frauke, Marcus Elvert, Boris P. Koch, Matthias Witt, and Kai-Uwe Hinrichs. 2009. "Molecular characterization of dissolved organic matter in pore water of continental shelf sediments." *Geochimica et Cosmochimica Acta* 73(11):3337–3358.
- Schneider, Julia, Guido Grosse, and Dirk Wagner. 2009. "Land cover classification of tundra environments in the Arctic Lena Delta based on Landsat 7 ETM+ data and its application for upscaling of methane emissions." *Remote Sensing of Environment* 113(2):380–391.
- Schuur, Edward a. G. et al. 2008. "Vulnerability of Permafrost Carbon to Climate Change: Implications for the Global Carbon Cycle." *BioScience* 58(8):701.
- Schwamborn, Georg, Volker Rachold, and Mikhail N Grigoriev. 2002. "Late Quaternary sedimentation history of the Lena Delta." *Quaternary International* 89(1):119–134.
- Serreze, MC, JE Walsh, FS Chapin, and T Osterkamp. 2000. "Observational evidence of recent change in the northern high-latitude environment." *Climatic Change* 159–207.

- Smith, Laurence C., and Tamlin M. Pavelsky. 2008. "Estimation of river discharge, propagation speed, and hydraulic geometry from space: Lena River, Siberia." *Water Resources Research* 44(3):1–11.
- Stuiver, M, and HA Polach. 1977. "Reporting of 14C data." *Radiocarbon* 19(3).
- Tarnocai, C. et al. 2009. "Soil organic carbon pools in the northern circumpolar permafrost region." *Global Biogeochemical Cycles* 23(2):1–11.
- Tsuyuzaki, Shiro, Tomoko Nakano, Shun-ichi Kuniyoshi, and Masami Fukuda. 2001. "Methane Flux in grassy marshlands near Kolyma River , north-eastern Siberia." 33:1419–1423.
- Wagner, D, S Kobabe, E.-M Pfeiffer, and H.-W. Hubberten. 2003. "Microbial controls on methane fluxes from a polygonal tundra of the Lena Delta, Siberia." *Permafrost and Periglacial Processes* 14(2):173–185.
- Walter, K M, S a Zimov, J P Chanton, D Verbyla, and F S Chapin. 2006. "Methane bubbling from Siberian thaw lakes as a positive feedback to climate warming." *Nature* 443(7107):71–5.
- Wille, Christian, Lars Kutzbach, Torsten Sachs, Dirk Wagner, and Eva-Maria Pfeiffer. 2008. "Methane emission from Siberian arctic polygonal tundra: eddy covariance measurements and modeling." *Global Change Biology* 14(6):1395–1408.
- Williams, PM, and LI Gordon. 1970. "Carbon-13: carbon-12 ratios in dissolved and particulate organic matter in the sea." Pp. 19–27 in *Deep Sea Research and Oceanographic Abstracts*, vol. 17. Elsevier.
- Yang, Daqing. 2002. "Siberian Lena River hydrologic regime and recent change." *Journal of Geophysical Research* 107(D23):1–10.
- Zhang, T, RG Barry, K Knowles, J.A. Heginbottom, and J Brown. 1999. "Statistics and characteristics of permafrost and ground-ice distribution in the Northern Hemisphere." *Polar Geography* 23(2):132–154.
- Zhulidov, A V, J V Headley, R D Robarts, and M J Brannen. 1997. *Atlas of Russian wetlands : biogeography and metal concentrations*. Saskatoon: National Hydrology Research Institute.
- Zimov, S. et al. 1997. "North Siberian Lakes: A Methane Source Fueled by Pleistocene Carbon." *Science* 277(5327):800–802.

## Appendix

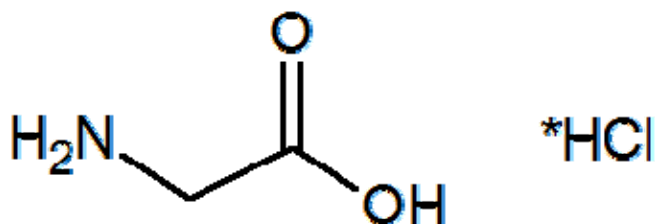
### Chemical structures and properties of standards

oxalic acid



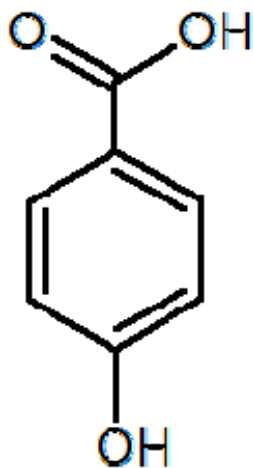
$C_2H_2O_4$   
M = 90.03 g/mol  
H:C = 1  
O:C = 2

glycine hydrochloride



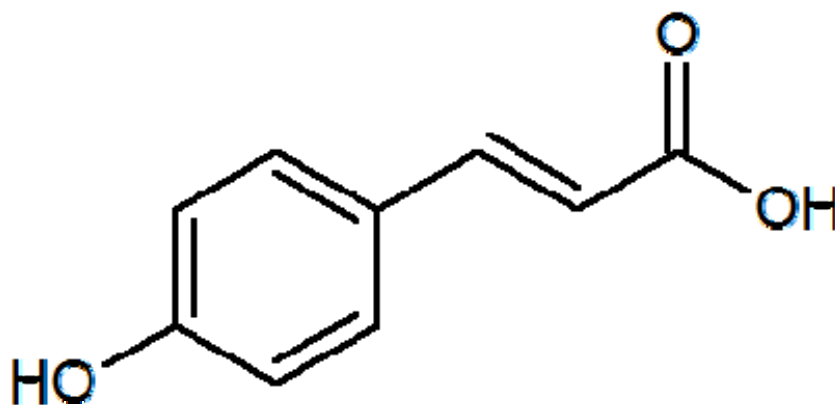
$C_2H_6NO_2 \cdot HCl$   
M = 111.53 g/mol  
H:C = 3  
O:C = 1

4-hydroxybenzaldehyde



$C_7H_6O_3$   
M = 138.12 g/mol  
H:C = 0.86  
O:C = 0.43

*p*-coumaric acid



$C_9H_8O_3$   
M = 164.16 g/mol  
H:C = 0.89  
O:C = 0.33

## UV-system construction plan

### Photochemical reactor and heat exchanger

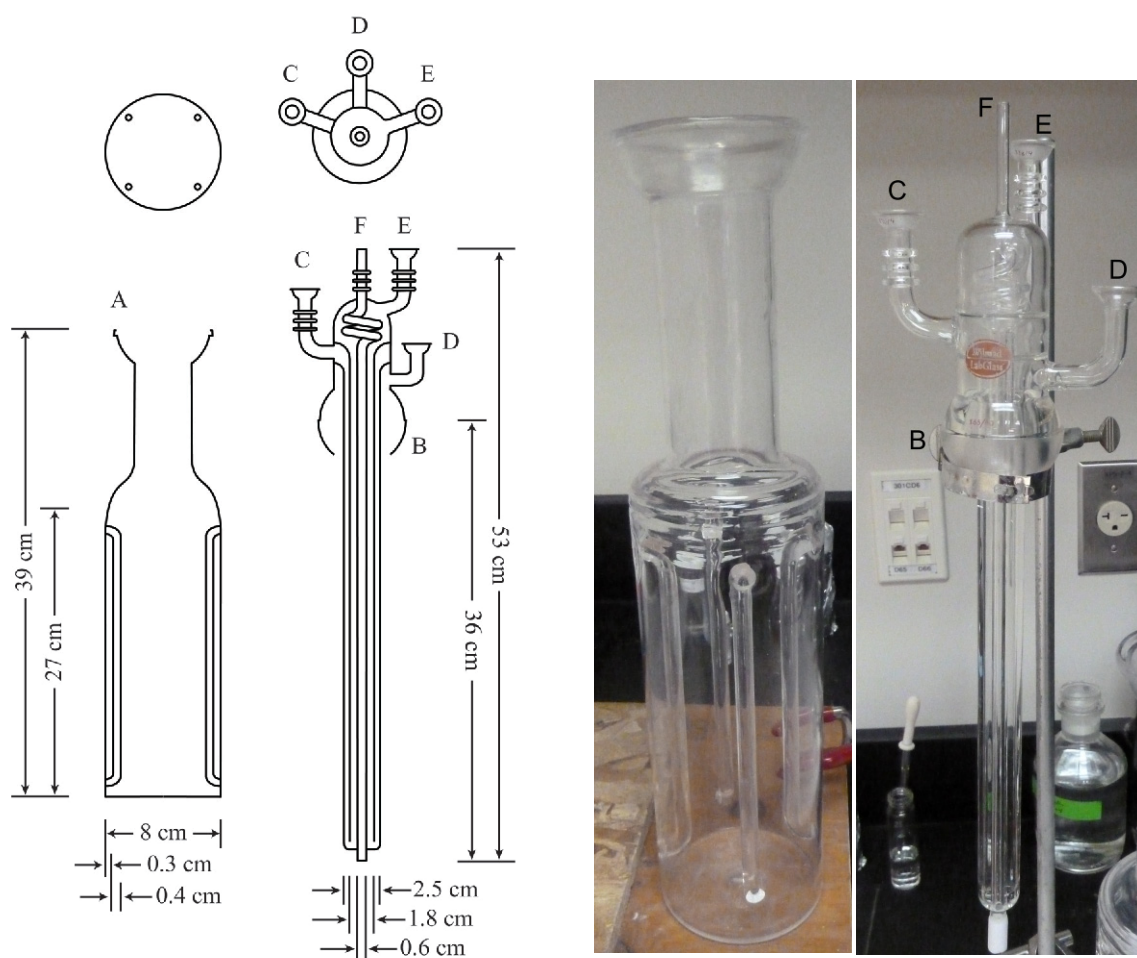


**Fig. A-1: Construction plans (left) and pictures (right) of the photochemical reactor and heat exchanger. Quartz reactor body (bottom left, middle right) with a cross-section view (top left) showing the baffle rod positions. Pyrex heat exchanger (bottom middle left, right) with an overhead view (top middle left) illustrating locations of the C) cold-water return; D) vent to vacuum line; E) cold-water supply 18/9 SJ sockets. Other components include the A) 65/40 SJ socket; B) 65/40 SJ ball member; and F) helium supply connection. Construction plans and description from *Beaupré et al.* [2007].**

## UV-lamp and reflector

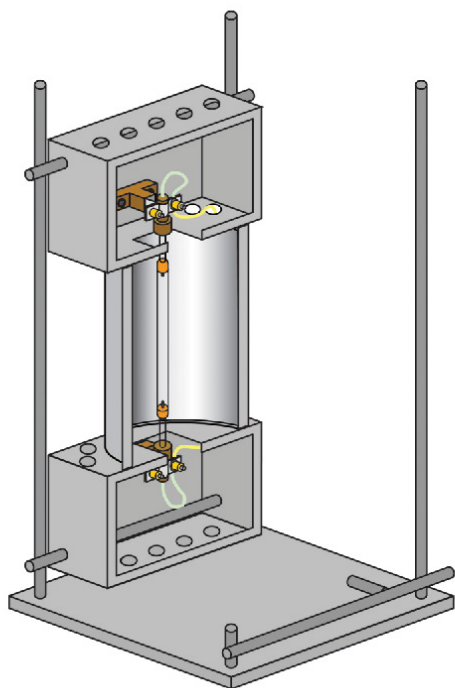


**Fig. A- 2: Construction plan (left) and picture of the UV-lamp and reflector. The assembly is mounted on an aluminium stand with four 1.3cm OD vertical support rods anchored into the vertices of a 24x24x1.3cm base plate. Two of these rods support the reflector using lattice connector clamps (*Chemglass Inc*, not shown), one supports the neck of the reactor with a three-pronged clamp, and the fourth supports a framework to precisely align and restrain the magnetic spin plate (not shown) upon which the reactor rests. Ceramic stand-offs and the ceramic end-fittings of the lamp are shown in brown. Construction plan and description from *Beaupré et al.* [2007].**

## Reactor chamber

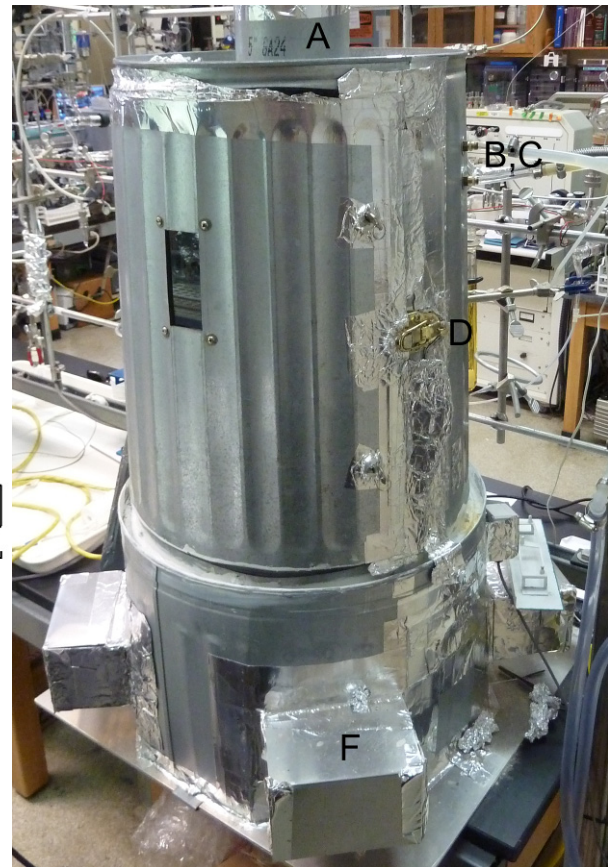
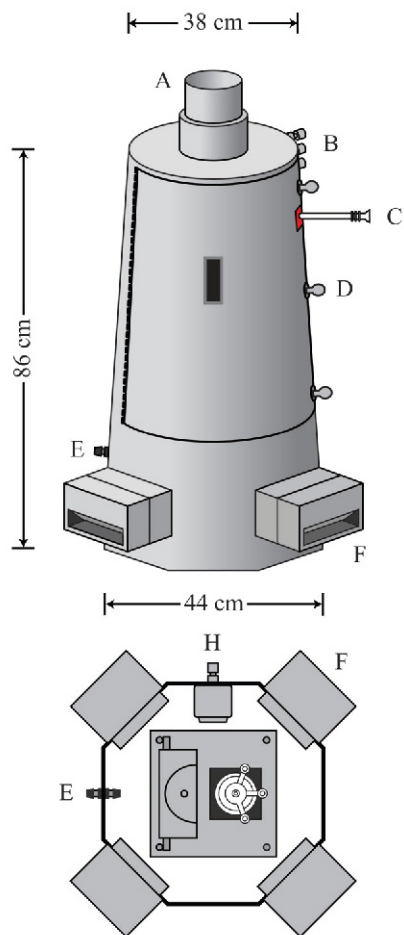


**Fig. A-3: Construction plan (left) and picture (right) of the reactor chamber.** A) exhaust duct coupling; B) bulkhead fittings for cooling water supply/return lines and helium supply line; C) 12 mm OD Pyrex tubing connecting the reactor to DOC vacuum line via an 18/9 SJ with 3 mairias, breaching the cabinet via a silicone flange (shown red); D) one of three pawl latches securing the curved door, hinged on the left hand side; E) bulkhead fitting for UV- lamp power lines; F) light-reducing baffled air intakes; G) cross-section of F, illustrating the tightly folded path that cooling air must travel; H) electrical outlet box and bulkhead fitting. Construction plan and description from *Beaupré et al.* [2007].

## Vacuum-line (VLUV)

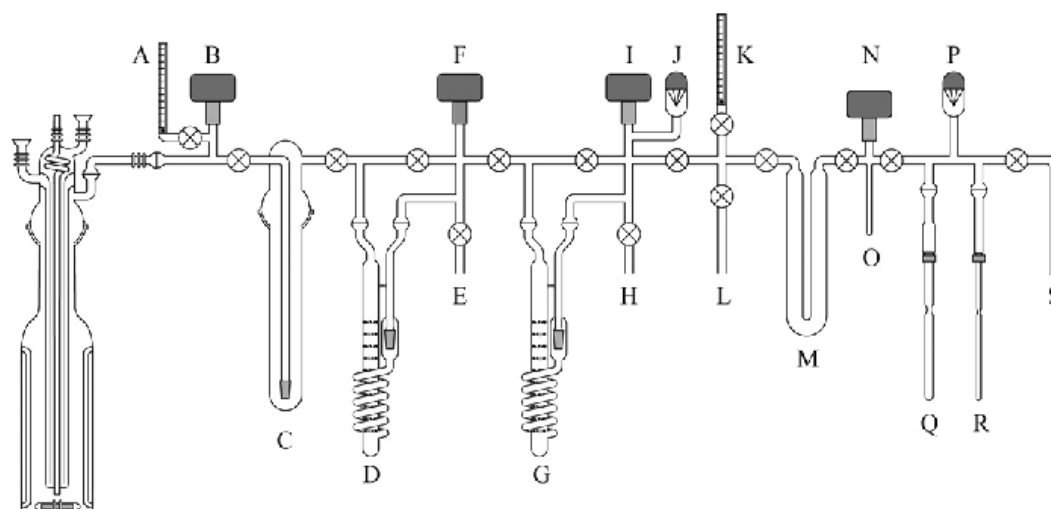


Fig. A- 4: Principle construction plan of the UV vacuum line. The use vacuum line was slightly modified, see text for detailed functional description. The majority of the line is manufactured from 12mm OD standard wall *Pyrex* tubing, sectioned by 4mm bore all-glass high vacuum stopcocks (*QBI Corp.*). Individual components are connected by spherical joints with *Viton* o-rings. A) flow meter #1; K) flow meter #2; B), F), I), N) capacitance manometers; J), P) thermocouple pressure gauge sensors; C) KI solution trap; D) modified Horibe trap #1 (dry ice/isopropanol slush bath); G) modified Horibe trap #2 (liquid nitrogen bath); M) U-tube trap; O) calibrated volume with a 7mm OD, 7cm long cold-finger; Q), R) break seal tubes for  $^{14}\text{C}$  and  $^{13}\text{C}$  splits, respectively, secured by internally-threaded o-ring adapters with *Teflon* bushings; E), H), L), and S) are conduits of a manifold (not shown for clarity) leading to the vacuum pump. Construction plan and description from *Beaupré et al.* [2007].

Method	Material	V <sub>sample</sub> <sup>1</sup> [mL]	C <sub>initial</sub> <sup>2</sup> [μMC]	n <sub>initial</sub> <sup>3</sup> [μmolC]	T <sub>CF</sub> <sup>4</sup> [°C]	p <sub>CF</sub> <sup>4</sup> [mbar]	V <sub>CF</sub> <sup>4</sup> [mL]	n <sub>CO2</sub> <sup>5</sup> [μmolC]	EE <sup>6</sup> [%]	n <sub>b</sub> <sup>7</sup> [μmolC]	n <sub>CO2_bc</sub> <sup>8</sup> [μmolC]	EE <sub>bc</sub> <sup>8</sup> [%]	Vacuum <sup>9</sup> Line
SPE	oxalic acid (1)	20	371.6	7.43	23.9	0.74	16.41	0.49	6.6	0.87	0.00	0	VLWH
	oxalic acid (2)	20	371.6	7.43	24.5	0.06	16.41	0.04	0.5	0.87	0.00	0	VLWH
	glycine hydrochloride (1)	20	358.9	7.18	24.5	0.89	16.41	0.59	8.2	0.87	0.00	0	VLWH
	glycine hydrochloride (2)	20	358.9	7.18	24.5	1.87	16.41	1.24	17.3	0.87	0.37	5.2	VLWH
	4-hydroxybenzaldehyde (1)	20	475.3	9.51	25	61.6	3.265	8.10	85.2	0.87	7.24	76.1	VLH
	4-hydroxybenzaldehyde (2)	20	475.3	9.51	24.2	52.8	3.265	6.96	73.3	0.87	6.10	64.1	VLH
	<i>p</i> -coumaric acid (1)	17.7	583.7	10.33	24	73.2	3.265	9.66	93.5	0.87	8.80	85.1	VLH
	<i>p</i> -coumaric acid (2)	18.6	583.7	10.86	23.6	78.2	3.265	10.34	95.2	0.87	9.47	87.2	VLH
	Cow Creek (1)	20	606.5	12.13	24.7	14.1	16.41	9.33	76.9	0.87	8.47	69.8	VLWH
	Cow Creek (2)	20	606.5	12.13	23.5	14.3	16.41	9.50	78.3	0.87	8.64	71.2	VLWH
UV	oxalic acid (1)	17.0	387.5	6.59	23.8	6.32	29.38	7.51	114.0	0.68	6.83	103.7	VLUV
	oxalic acid (2)	18.2	387.5	7.05	24.1	5.85	29.38	6.95	98.5	0.68	6.26	88.8	VLUV
	glycine hydrochloride (1)	18.1	356.0	6.44	23.9	6.43	29.38	7.64	118.6	0.68	6.96	108.0	VLUV
	glycine hydrochloride (2)	18.5	355.9	6.58	23.8	6.24	29.38	7.42	112.6	0.68	6.73	102.3	VLUV
	Cow Creek (1)	18.7	606.5	11.34	23.5	10.24	29.38	12.18	107.4	0.68	11.50	101.4	VLUV
	Cow Creek (2)	19.2	606.5	11.64	23.9	10.24	29.38	12.17	104.5	0.68	11.48	98.6	VLUV

Method	Material	V <sub>sample</sub> <sup>1</sup> [mL]	C <sub>initial</sub> <sup>2</sup> [μMC]	n <sub>initial</sub> <sup>3</sup> [μmolC]	T <sub>CF</sub> <sup>4</sup> [°C]	p <sub>CF</sub> <sup>4</sup> [mbar]	V <sub>CF</sub> <sup>4</sup> [mL]	n <sub>CO2</sub> <sup>5</sup> [μmolC]	EE <sup>6</sup> [%]	n <sub>b</sub> <sup>7</sup> [μmolC]	n <sub>CO2_bc</sub> <sup>8</sup> [μmolC]	EE <sub>bc</sub> <sup>8</sup> [%]	Vacuum <sup>9</sup> Line
RV	oxalic acid (1)	20	371.6	7.43	23.5	5.98	16.41	3.97	53.5	0.16	3.82	51.3	VLWH
	oxalic acid (2)	20	371.6	7.43	24.3	8.76	16.41	5.81	78.1	0.16	5.65	76.0	VLWH
	glycine hydrochloride (1)	20	358.9	7.18	25.3	8.86	16.41	5.85	81.5	0.16	5.69	79.3	VLWH
	glycine hydrochloride (2)	20	358.9	7.18	23.5	9.02	16.41	5.99	83.5	0.16	5.84	81.3	VLWH
	glycine hydrochloride (3)	35	460	16.10	22.8	114.2	3.265	15.14	94.0	0.16	14.98	93.0	VLH
	glycine hydrochloride (4)	14.7	460	6.76	23.4	47.7	3.265	6.31	93.3	0.16	6.15	91.0	VLH
	Cow Creek (1)	20	606.5	12.13	24.2	10.23	16.41	6.78	55.9	0.16	6.62	54.6	VLWH
	Cow Creek (2)	20	606.5	12.13	25	6.79	37.17	10.17	83.8	0.16	10.01	82.5	VLWH
	L11-06	14.9	823.3	12.27	25	97.7	3.265	12.85	104.8	0.16	12.69	103.5	VLH
	L11-07-03	14.5	820.4	11.90	n.a.	n.a.	n.a.	n.a.	n.a.	n.a.	n.a.	n.a.	
	L11-08/09	29.2	833.1	24.33	23.2	162.2	3.265	21.47	88.2	0.16	21.31	87.6	VLH
	L11-10/11	32.8	838.0	27.49	24.2	191.7	3.265	25.29	92.0	0.16	25.13	91.4	VLH
	L11-12/13	34.1	813.9	27.75	24	198.6	3.265	26.21	94.5	0.16	26.06	93.9	VLH
	L11-14/15	35.5	792.8	28.14	22.8	195.0	3.265	25.84	91.8	0.16	25.69	91.3	VLH

Tab. A- 1: Summary of all processed standards and samples, including all variables and results of the manometric CO<sub>2</sub> quantification and blank correction.

<sup>1</sup>Initial sample volume; <sup>2</sup>Initial sample DOC concentration; <sup>3</sup>Initial amount of DOC; <sup>4</sup>Temperature, pressure, and volume of the cold-finger during manometric CO<sub>2</sub> quantification; <sup>5</sup>Quantified amount of CO<sub>2</sub>, calculated according to Eq. 4; <sup>6</sup>Extraction efficiency calculated according to Eq. 5; <sup>7</sup>Amount of blank carbon incorporated during sample processing; <sup>8</sup>Blank-corrected amount of quantified CO<sub>2</sub> and corresponding blank-corrected extraction efficiency; <sup>9</sup>Vacuum line used for CO<sub>2</sub> quantification.

Key: SPE, solid phase extraction; UV, ultraviolet-oxidation; RV, roto-evaporation; VLWH, vacuum-line system at NOSAMS; VLH; vacuum-line system at IUP, Heidelberg; VLUV, vacuum-line at the UV-system at NOSAMS.

## Error Analysis

The total uncertainty of the blank-corrected values using Eq.8 can be calculated by the following equation (Eq. A-I) [Hwang & Druffel 2005]:

$$\begin{aligned}
 (\partial fMC_{smp})^2 &= \left( \frac{\partial fMC_{smp}}{\partial fMC_{smp+b}} \right)^2 (\partial fMC_{smp+b})^2 + \left( \frac{\partial fMC_{smp}}{\partial fMC_{std+b}} \right)^2 (\partial fMC_{std+b})^2 + \left( \frac{\partial fMC_{smp}}{\partial fMC_{std}} \right)^2 (\partial fMC_{std})^2 \\
 &+ \left( \frac{\partial fMC_{smp}}{\partial m_{smp+b}} \right)^2 (\partial m_{smp+b})^2 + \left( \frac{\partial fMC_{smp}}{\partial m_{std+b}} \right)^2 (\partial m_{std+b})^2 + \left( \frac{\partial fMC_{smp}}{\partial m_b} \right)^2 (\partial m_b)^2
 \end{aligned}$$

where  $fMC$  is the fraction modern carbon, can be substituted by  $\Delta^{14}C$  (or  $\delta^{13}C$ ),  $m$  is the mass and the subscribes  $smp$ ,  $std$  and  $b$  are sample, standard and blank, respectively.

Individual terms in Eq. A-I are calculated as follows:

$$\frac{\partial fMC_{smp}}{\partial fMC_{smp+b}} = \frac{m_{smp+b}}{m_{smp+b} - m_b} \quad (A-II)$$

$$\frac{\partial fMC_{smp}}{\partial fMC_{smp+b}} = \frac{-m_{smp+b}}{m_{smp+b} - m_b} \quad (A-III)$$

$$\frac{\partial fMC_{smp}}{\partial fMC_{std}} = \frac{m_{std+b} - m_b}{m_{smp+b} - m_b} \quad (A-IV)$$

$$\left( \frac{\partial fMC_{smp}}{\partial m_{smp+b}} \right) = \frac{-m_b \times (fMC_{smp+b} - fMC_{std}) + m_{std+b} \times (fMC_{std+b} - fMC_{std})}{(m_{smp+b} - m_b)^2} \quad (A-V)$$

$$\frac{\partial fMC_{smp}}{\partial m_{std+b}} = \frac{-fMC_{std+b} + fMC_{std}}{m_{smp+b} - m_b} \quad (A-VI)$$

$$\frac{\partial fMC_{smp}}{\partial m_b} = \frac{m_{smp+b} \times (fMC_{smp+b} - fMC_{std}) - m_{std+b} \times (fMC_{std+b} - fMC_{std})}{(m_{smp+b} - m_b)^2} \quad (A-VII)$$

**Declaration acc. To § 22 Abs. 9 Allg. Teil d. Master-PO**

I hereby declare that I wrote my Master thesis independently and that I did not use other sources and auxiliary means than the ones indicated.

I further declare that the Master thesis **might be** made available to the public in this version.

Place/Date: Bremen, 12<sup>th</sup> of November 2012

Signature: \_\_\_\_\_

Hendrik Grotheer